Spin Crossover and Fluorine-Specific Interactions in Metal Complexes of Terpyridines with Polyfluorocarbon Tails

Maite Nößler,[a] Nicolás I. Neuman,[b, c] Lisa Böser,[a] René Jäger,[a] Arijit Singha Hazari,[b] David Hunger,[d] Yixian Pan,[d] Clemens Lücke,[b] Tobias Bens,[b] Joris van Slageren,*[d] and Biprajit Sarkar*[a, b]

Abstract: In coordination chemistry and materials science, terpyridine ligands are of great interest, due to their ability to form stable complexes with a broad range of transition metal ions. We report three terpyridine ligands containing different perfluorocarbon (PFC) tails on the backbone and the corresponding Fe^{II} and Co^{II} complexes. The Co^{II} complexes display spin crossover close to ambient temperature, and the nature of this spin transition is influenced by the length of the PFC tail on the ligand backbone. The electrochemical properties of the metal complexes were investigated with cyclic voltammetry revealing one oxidation and several reduction processes. The fluorine-specific interactions were investigated

by EPR measurements. Analysis of the EPR spectra of the complexes as microcrystalline powders and in solution reveals exchange-narrowed spectra without resolved hyperfine splittings arising from the ^{59}Co nucleus; this suggests complex aggregation in solution mediated by interactions of the PFC tails. Interestingly, addition of perfluoro-octanol in different ratios to the acetonitrile solution of the sample resulted in the disruption of the F···F interactions of the tails. To the best of our knowledge, this is the first investigation of fluorine-specific interactions in metal complexes through EPR spectroscopy, as exemplified by exchange narrowing.

Introduction

In the last decades, 2,2′:6′,2′′-terpyridines have become popular ligands in coordination chemistry due to their ability to form stable complexes with different transition-metal ions.[1] The synthesis of 2,2′:6′,2′′-terpyridine and its derivatives has been extensively studied for the past decades. However, there are limitations regarding the synthesis of new terpyridine ligands, especially those bearing electronically different sub-

stituents on the pyridine units.[2] The metal complexes bearing terpyridine ligands were investigated for various applications as photosensitizers,[3] gel systems,[4] ion sensors,[5] supramolecular polymers,[6] redox shuttles for dye sensitized solar cells (DSSC),[7] and catalysis for proton and CO_2 reduction[8] and water oxidation.[9]

Moreover, metal-terpyridine complexes were reported to exhibit spin-crossover behavior. Spin-crossover (SCO), first described in the 1930s by Cambi et al.,[10] usually occurs in d^n ($n = 4$–7) transition metal complexes providing transitions between the high-spin (HS) and low-spin (LS) states.[11] This phenomenon is most commonly observed in Co^{II} and Fe^{II} complexes.[12]

Because of their potential use in information storage, sensors, electro-optical devices and spintronics, multifunctional molecular materials (materials that exhibit synergistic coexistence of two or more properties) are currently popular.[13] Among these, liquid crystals (LC) are considered as fascinating functional materials.[14] Metallomesogens, liquid crystals of transition metal complexes, which show multi-functionality (spin-crossover, mixed-valence etc.), have attracted significant attention due to the co-occurrence of physical properties (magnetic, optical and electrical properties).[14,15] A new class of functional materials was found as SCO metallomesogens, where LC properties and SCO are synchronized.[14–16] In addition, other multifunctional molecule-based materials are SCO compounds that are coupled with nonlinear optical (NLO)[17] and/or luminescence properties.[18]

One way to control SCO properties and the cooperativity in such molecules is the introduction of long alkyl chains.[19] Along this line, Hayami and co-workers reported a number of

[a] M. Nößler, L. Böser, R. Jäger, Prof. Dr. B. Sarkar
Institut für Chemie und Biochemie
Freie Universität Berlin
Fabeckstraße 34–36, 14195, Berlin (Germany)
E-mail: biprajit.sarkar@iac.uni-stuttgart.de
Homepage: http://www.iac.uni-stuttgart.de/en/research/aksarkar/

[b] Dr. N. I. Neuman, Dr. A. Singha Hazari, C. Lücke, T. Bens, Prof. Dr. B. Sarkar
Institut für Anorganische Chemie, Universität Stuttgart
Pfaffenwaldring 55, 70569 Stuttgart (Germany)

[c] Dr. N. I. Neuman
Instituto de Desarrollo Tecnológico para la Industria Química
INTEC, UNL-CONICET Predio CCT Conicet "Dr. Alberto Cassano"
Colectora RN 168, Km 0, Paraje El Pozo
3000 Santa Fe (Argentina)

[d] D. Hunger, Y. Pan, Prof. Dr. J. van Slageren
Institut für Physikalische Chemie, Universität Stuttgart
Pfaffenwaldring 55, 70569 Stuttgart (Germany)
E-mail: slageren@ipc.uni-stuttgart.de

Chem. Eur. J. **2023**, *29*, e202301246 (1 of 15)

© 2023 The Authors. Chemistry - A European Journal published by Wiley-VCH GmbH

Chemistry–A European Journal

Research Article
doi.org/10.1002/chem.202301246

**Chemistry
Europe**
European Chemical
Societies Publishing

terpyridine Co-complexes containing long alkyl chains displaying interesting magnetic and LC properties.[11,14,19a,20] The alkylated cobalt complexes published from the group of Hayami displayed not only "reverse spin transition" between the HS and LS state,[10] but also abrupt,[14] multi-phase[21] and gradual SCO[19a] properties. Additionally, a structural phase transition was shown to trigger a thermal hysteresis loop.[10] The flexibility of these complexes can directly influence cooperative interactions through structural changes, or indirectly, through random packing structure, and therefore play an important role in the aforementioned magnetic properties.[10,19a]

In general, per- and polyfluoroalkyl substances (PFAS) are extremely stable physically, chemically and biologically, due to the carbon-fluorine bond, which results in a high resistance to degradation and a high potential of bioaccumulation.[22] Furthermore, their use in a variety of industrial applications and consumer products has led to widespread global contamination.[23] However, the area of research of fluorine chemistry is continuously developing, as there are various applications for metal complexes with perfluorocarbon (PFC) tails such as in catalysis, supramolecular chemistry, synthesis and separation technologies and novel technological developments.[9] Therefore, the use of perfluorinated alkyl chains is very interesting, but only a handful of examples of metal complexes bearing fluorous tails exist in the literature.[4,9] Usually, these systems were mostly investigated towards their gelation properties, as the perfluorinated compounds are typically lipophobic and hydrophobic at the same time and therefore show self-assembly behavior.[4,24] The self-assembly can be controlled not only by H-bonds but also by halogen bonding (between appropriate partners) and weak interactions, like fluorine-fluorine (F⋯F) interactions,[24] which can also be of great significance for hysteretic SCO behavior.[25]

Electron paramagnetic resonance (EPR) is a widely used technique to investigate radical species. One phenomenon observed in EPR is exchange narrowing, first suggested by Gorter and Van Vleck.[26] Exchange narrowing can be due to chemical interconversion between species with different magnetic parameters, for example caused by thermal motion of atoms in liquids and some solids, or due to exchange interaction between the unpaired spins in different paramagnetic centers in an extended system.[26–27] Different mathematical methods were developed to model the narrowing of the resonance lines.[28] In diluted systems the line shape can be influenced by dipole-dipole interactions between paramagnetic centers,[28c,29] as well as partially resolved fine and hyperfine splittings. Meanwhile, in magnetically undiluted systems the isotropic exchange interaction may be dominant, resulting in a single resonance for each magnetic field orientation, with a linewidth determined by the interplay of exchange narrowing and the broadening produced by all anisotropic magnetic interactions (anisotropic exchange, dipolar interaction and hyperfine splittings, for example).[30] The narrowing effect is mediated by an exchange frequency, related to the exchange parameter J, coupling the magnetic centers of neighboring molecules. If the exchange frequency is much smaller than the hyperfine splittings in each magnetic center, a well resolved spectrum may be observed. As the exchange interactions increase, the individual resonance lines broaden and merge into the "gravity center" of the spectra. Finally, if the exchange is larger than the separation between individual resonances, a single resonance is obtained, which becomes narrower with the increase of J.[31] To the best of our knowledge, exchange narrowing has not been investigated in the context of molecular aggregation mediated by fluorine-specific interactions (weak noncovalent interactions involving at least one F unit).
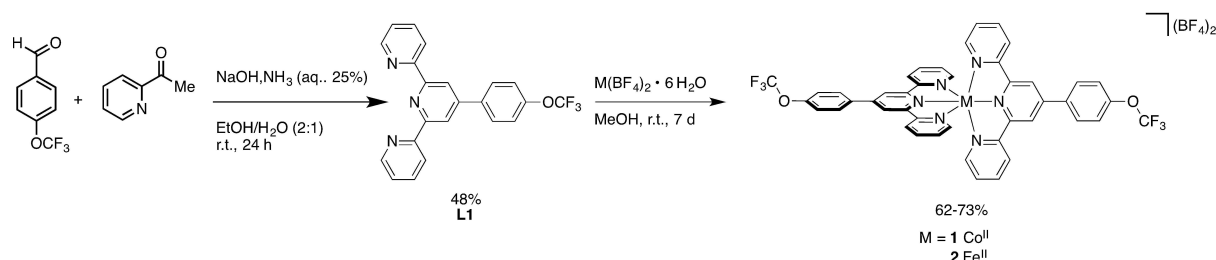
As part of our recent interest in metal complexes of fluorinated terpyridine ligands,[32] we report here on several complexes of iron and cobalt centers containing terpyridine ligands with PFC tails (Figure 1). These complexes were investigated through SQUID magnetometry with a focus on SCO behavior. Furthermore, the exchange narrowing in the EPR spectra was investigated towards F⋯F interactions of the PFC tails. Regarding this, also DFT calculations were performed.

Results and Discussion

Synthesis, crystal structures and magnetic properties

The ligands were synthesized by adapting previously published routes.[4,33] The ligand **L1** was synthesized according to a known synthetic route for terpyridine ligands (Scheme 1).[33]

The ligands **L2** and **L3** were synthesized over two different routes by adding either 3,3,4,4,5,5,6,6,7,7,8,8,8-tridecafluorooctyl trifluoromethanesulfonate (R$_f$Oct-OTf) or 3,3,4,4,5,5,6,6,7,7,8,8,9,9,10,10,10-heptadecafluorodecyl tri-

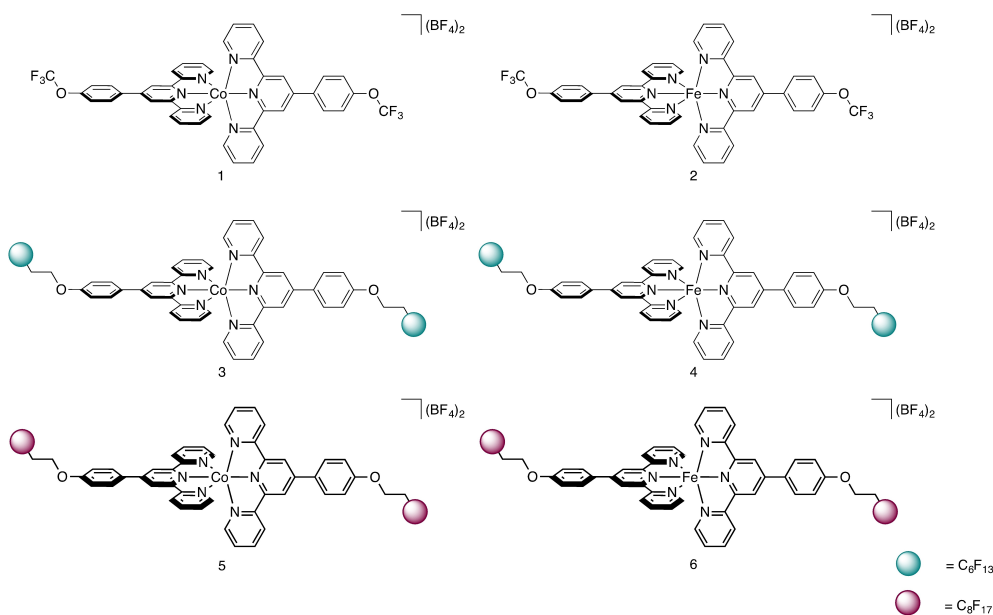**Scheme 1.** Synthesis of ligand **L1** and complexes **1** and **2**.

Chemistry–A European Journal

Research Article
doi.org/10.1002/chem.202301246

**Chemistry
Europe**
European Chemical
Societies Publishing

Figure 1. Terpyridine containing complexes with Co^{II} and Fe^{II} metal centers.

fluoromethanesulfonate (R$_f$Dec-OTf) to a basic solution of 2,2′:6′,2′′-terpyridin-4′-ol (route 1, Scheme 2) or 4-hydroxyaldehyde (route 2, Scheme 2) under basic conditions in acetone.[4] The aldehyde was further reacted to the corresponding terpyridine ligand. These ligands were then used to synthesize the respective iron or cobalt metal complexes.

All complexes were purified by precipitating a solution of the complexes in acetonitrile with diethyl ether. The ligands as well as the complexes were characterized by NMR spectroscopy, mass spectrometry and elemental analysis.

For complexes **1**, **2** and **5**, suitable single crystals for X-ray diffraction analysis were obtained (Figures 2 and 3). While the data for other complexes were not of sufficient quality to
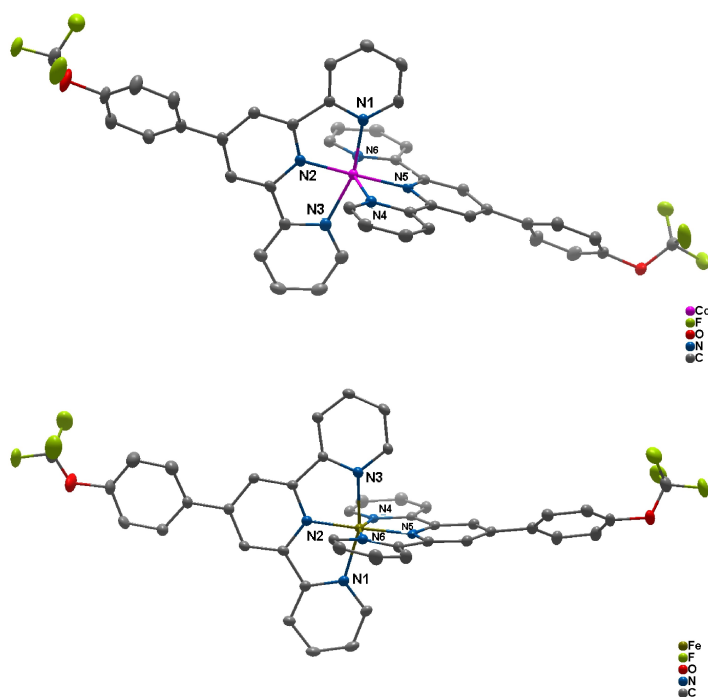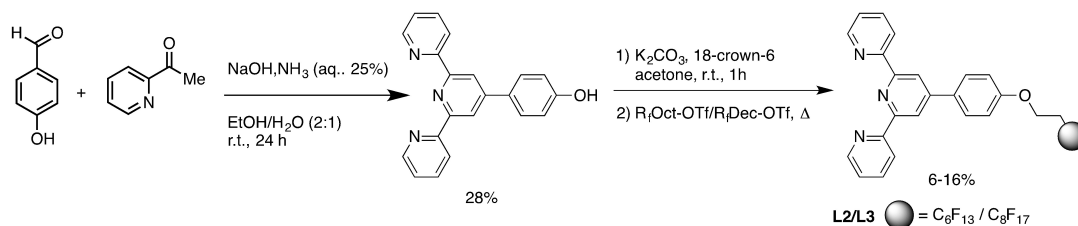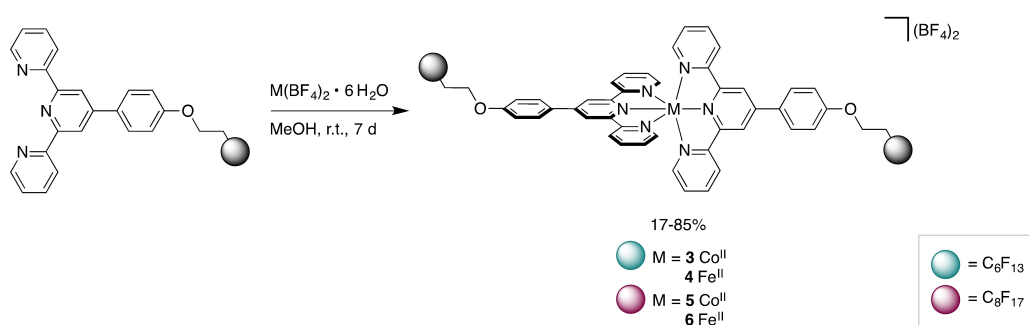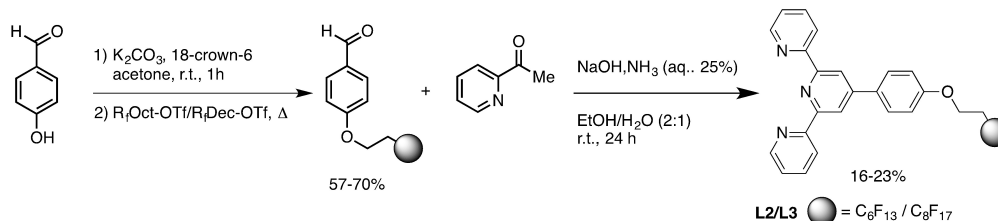

Figure 2. Perspective view of cobalt complex **1** (top) and iron complex **2** (bottom). Ellipsoids are at a probability level of 50%. H atoms, anions and solvent molecules are omitted for clarity.

Chemistry–A European Journal

Research Article
doi.org/10.1002/chem.202301246

Chemistry Europe
European Chemical
Societies Publishing

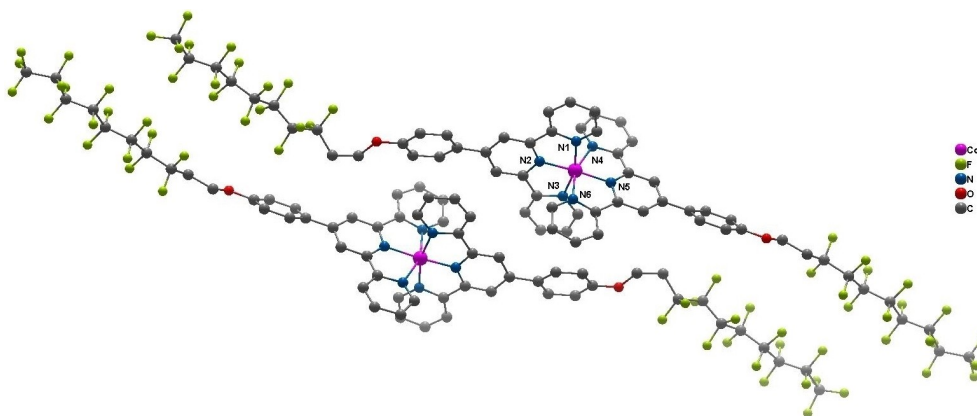**Scheme 2.** Synthesis of ligands **L2** and **L3** and complexes **3–6**.

Figure 3. Perspective view of cobalt complex **5**. Ellipsoids are at a probability level of 50%. H atoms, anions and solvent molecules are omitted for clarity.

obtain good solid-state structures, as the complexes crystallize in small plates leading to a broad range of difficulties during the refinement processes. In this regard, there is precedence that crystallizing compounds with long fluorous tails is comparatively complicated.[9] In spite of that, the data of complex **5** was of sufficient quality to prove the desired connectivity, intermolecular interactions and the discussion of the metal-ligand distances.

Complexes **1** and **2** crystallize in the triclinic $P\bar{1}$ space group and show the expected coordination motif: three nitrogen atoms of each ligand coordinate in a distorted octahedral fashion to the metal center. The phenyl rings with the PFC tag on the backbone are twisted out of the plane of the terpyridine unit. Selected bond lengths are depicted in Table 1. The bond lengths between 1.874 (2) and 2.144 (2) Å, indicate a LS Co^{II} center in the complexes **1** and **5**.[34] Similarly,

Chemistry–A European Journal

Research Article
doi.org/10.1002/chem.202301246

**Chemistry
Europe**
European Chemical
Societies Publishing

Table 1. Selected bond lengths of complexes **1**, **2** and **5** in Å.

	M–N1	M–N2	M–N3	M–N4	M–N5	M–N6
1	2.000(2)	1.874(2)	2.013(2)	2.136(2)	1.921(2)	2.144(2)
2	1.973(2)	1.875(2)	1.975(2)	1.962(2)	1.874(2)	1.973(2)
5	1.980(9)	1.87(1)	1.99(1)	2.17(1)	1.93(1)	2.14(1)
Co[TPYOC$_{14}$H$_{29}$]$_2$ (BF$_4$)$_2$[20a],[a]	2.137(4)/	1.910(3)	2.114(4)	1.977(4)	1.844(3)	1.976(4)
Fe[N$_3$P$_3$(OPh)$_5$(OPhTPY)]$_2$(PF$_6$)$_2$[35],[b]	1.886(3)	1.987(3)	1.995(3)	1.878(4)	1.976(3)	1.979(4)

[a] Complex with a LS Co^{II} center. [b] Complex with a LS Fe^{II} center.

the bond lengths between 1.874 (2) and 1.975 (2) Å point towards a LS Fe^{II} center in complex **3**.[35] These measurements were carried out at 100 K.

The angle between the planes of the tridentate ligands are nearly perpendicular to one another with values of 87.1° for complex **1**, 85.8° for complex **2** and 89.2° for complex **5**. The packing of the complexes is as observed for previously reported complexes with terpyridine ligands.[32a,36] Packing diagram reveals face-to-face orientation of the terpyridine units, while the BF$_4^-$ anions and solvent molecules are found between the sheets (Figures S30 and S32 in the Supporting Information). In complexes **1** and **2** the OCF$_3$ tails are aligned with the OCF$_3$ groups of the neighboring molecule (Figures S31 and S34).

For the complexes described here, different spin states can exist and in principle reversible switching between these spin states by external stimuli can be possible. SQUID magnetometry is an excellent method to probe the temperature

dependent SCO behavior of Fe^{II} and Co^{II} compounds. If the energy difference between HS ($S = 2$ or $S = 3/2$, for Fe^{II} and Co^{II} respectively) and LS ($S = 0$ or $S = 1/2$) states is small, SCO can occur as a function of temperature due to the higher vibrational entropy of the HS state.[37] For this, complexes **1–6** were investigated by the means of SQUID magnetometry in the temperature (T) range of 1.8 to 300 K. The T dependence of the χT product is depicted in Figure 4, where χ is the molar static magnetic susceptibility, which at low fields can be approximated as the ratio between the molar magnetization and the applied magnetic field.

As can be seen from Figure 4, for the cobalt complex **1**, no SCO was observed, and the temperature dependence of the χT product hints towards the simultaneous existence of LS as well as HS Co^{II}. This is supported by the curvature at low temperatures, which indicates a significant ZFS. On the basis of the Curie Law, a χT of about 2 cm^3 K mol^{-1} at high temperatures for a $g_{iso} = 2.3$ is expected. The value of 0.75 cm^3 K mol^{-1} at
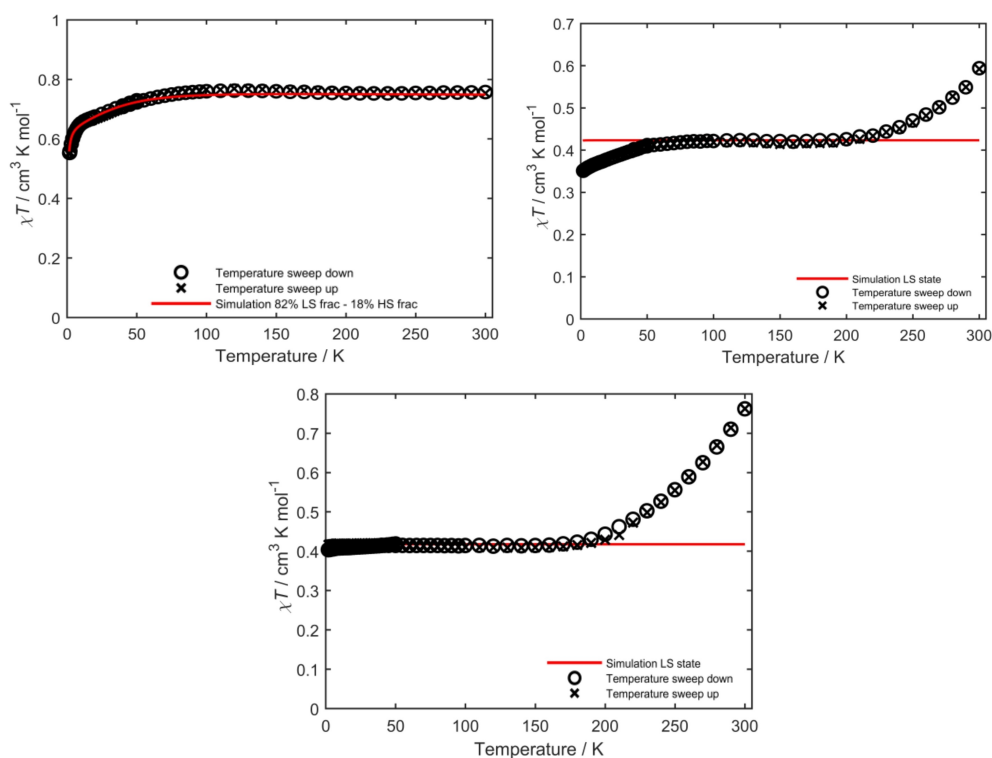

Figure 4. Temperature dependency of the $\chi_M T$ product for **1** (top left), **3** (top right) and **5** (bottom) in an applied magnetic field of 1000 Oe as well as the corresponding LS spin Hamiltonian simulations.

Chemistry–A European Journal

Research Article
doi.org/10.1002/chem.202301246

**Chemistry
Europe**
European Chemical
Societies Publishing

300 K is significantly lower than this, which is consistent with parallel existence of LS and HS state. Indeed, the obtained simulation was found to be in good agreement with the experimental data, if a composition of 18% HS state and 82% LS state is assumed. The spin Hamiltonian parameters for the LS species ($g_{x,y} = 2.08(2)$, $g_z = 2.15(2)$) are in good agreement with the values found by EPR. In the case of the HS species, values of $g_{x,y} = 2.0(1)$ and $g_z = 2.5(1)$ as well as zero-field splitting parameters of $D = -44(2)$ cm^{-1} and $E = 0.25(5)D$ were found. Additionally, the prominent decrease of $\chi_M T$ below 5 K might indicate towards a non-negligible intermolecular antiferromagnetic interaction. Following this assumption, the intermolecular coupling strength was quantified to be 0.17(3) cm^{-1}. A large contribution of the LS state is in agreement with the structural data described above, in which the Co–N bond lengths better better with a LS state of the Co^{II} center.

For complex **3** a gradual thermal SCO behavior is observed from 210 K onwards with increasing temperature. The $\chi_M T$ value for complex **3** increases from 0.35 cm^3 K mol^{-1} at 1.8 K to 0.42 cm^3 K mol^{-1} at 75 K and remains almost constant at 0.42 cm^3 K mol^{-1} up to 200 K. From 200 K, the start of the SCO is observed with a gradual increase of the $\chi_M T$ value from 0.42 cm^3 K mol^{-1} at 200 K to 0.6 cm^3 K mol^{-1} at 300 K.

Complex **5** displays a similar SCO behavior as complex **3**. In contrast the $\chi_M T$ value remains almost constant at 0.42 cm^3 K mol^{-1} with growing temperature, until it starts increasing upon heating at 200 K. The curve is gradually increasing up to 300 K with a $\chi_M T$ value of 0.76 cm^3 K mol^{-1}.

Spin-Hamiltonian simulations of the temperature dependence of $\chi_M T$ of **3** and **5** based on the parameters obtained by powder EPR of the LS species are displayed in Figure 4. While for **5**, the simulated $\chi_M T$ values between 5 and 100 K are in good accordance with the experimental data, a strong deviation in the case of **3** is found. In the case of **3**, the measured curve also shows a bending to smaller $\chi_M T$ values below 5 K, hinting towards an interaction, which is not covered by the simulation. An explanation for this is a residual of HS species at low temperatures, which is significantly higher in the case of **3** than it is for **5**. In the case of the three cobalt complexes investigated here, it is seen that the percentage of the HS form observed at ambient temperatures steadily increases with the size of the PFC tail on the terpyridine backbone.

In the case of Fe^{II} complexes, no SCO and a minor $\chi_M T$ value was observed from 1.8 up to 300 K. The LS state of Fe^{II} is $S = 0$ and hence it does not possess any magnetic moment. Nevertheless with 0.015, 0.0125 and 0.06 cm^3 K mol^{-1}, a non-zero value of $\chi_M T$ is found at 300 K. This is even lower than the theoretical value for a $S = \frac{1}{2}$ system with $g = 2$ (0.375 cm^3 K mol^{-1}). As in the case of all Fe^{II} compounds, this moment is attributed to a minor Fe^{II} HS amount in the sample (Figure S1), which we also observed in complexes that we investigated earlier.[32a]

Complexes **3–6** were investigated towards their liquid crystalline properties. However, none of the complexes show a phase transition under the POM in the temperature rate from room temperature to 350 °C, as the compounds stayed solid over the measured temperature range.

Cyclic voltammetry

In order to investigate the electrochemical properties of the complexes cyclic voltammetric measurements of complexes **1**–**6** were performed (Figure 5). The measurements were performed in a 0.1 M NBu$_4$PF$_6$ dichloromethane or acetonitrile solution. For most of the complexes only one oxidation process could be observed. For the cobalt complexes the first oxidation is reversible and similar to the potential of -0.07 V of the Co(TPY)$_2$$^{2+}$ [2a] complex (-0.11 for **1**; -0.16 V for **3** and -0.17 V for **5** in MeCN). The peak-to-peak separation for the first oxidation step is rather large for complex **1** with ΔE_p of 111 mV, while values of 79 mV for complex **3** and 75 mV for **5** were obtained. At ambient temperatures, these Co^{II} complexes are expected to exist in the HS state in solution (as indicated by the observed paramagnetic shift in NMR spectroscopy). Oxidation of the complexes is expected to result in a LS Co^{III} center. The large structural change required for this transformation likely demands a large reorganization energy, which is reflected in the large peak-to-peak separation for the oxidation steps of these complexes.

Compared to the cobalt complexes, the iron complexes display a strongly anodically shifted first oxidation step (Figure 5 and Table 2). The difference in the oxidation potentials on changing the metal center is likely related to the removal of an electron from a highly stabilized formally t$_{2g}$ orbital in LS Fe^{II} complexes. For the HS Co^{II} complexes an electron is removed from the destabilized e$_g$ orbitals, which requires less energy.

In contrast to the first oxidation step, the potentials for the first reduction step are anodically shifted for the Co^{II} complexes (**1**, **3** and **5**) in comparison to the Fe^{II} complexes (**2**, **4** and **6**). As has been reported earlier for similar systems, the first reduction step in such iron complexes is tpy centered and
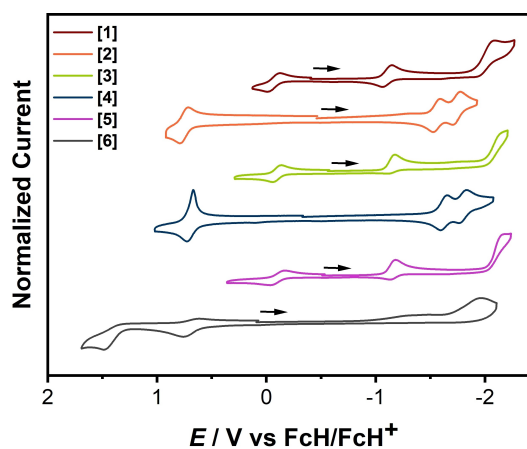
Figure 5. Cyclic voltammograms of complexes **1–6** in dichloromethane/NBu$_4$PF$_6$ measured with a glassy carbon working electrode; FcH = ferrocene, FcH$^+$ = ferrocenium.

Chemistry–A European Journal

Research Article
doi.org/10.1002/chem.202301246

Chemistry Europe
European Chemical
Societies Publishing

Table 2. Redox potentials versus FcH/FcH⁺ measured in acetonitrile at 100 mVs⁻¹ with 0.1 M Bu₄NPF₆ at room temperature.[a]

	Solvent	E_{fp}^{Ox2}	$E_{1/2}^{Ox1}$	$E_{1/2}^{Red1}$	$E_{1/2}^{Red2}$	$E_{1/2}^{Red3}$	$E_{1/2}^{Red4}$	E_{fp}^{Red5}	E_{fp}^{Red6}
1	MeCN	–	−0.11	−1.13	−1.93	−2.26	−2.59	–	–
2	MeCN	–	0.72	−1.57	−1.68	−2.30	−2.48	−2.63[b]	−3.12[b]
3	MeCN	–	−0.16[b]	−1.18	−2.01	−2.39[b]	–	–	–
4	MeCN	–	0.69	−1.41	−1.63[b]	−1.70[b]	−2.04[b]	−2.45[b]	–
5	MeCN	–	−0.17	−1.19	−2.02	−2.35	–	–	–
6	MeCN	–	0.68	−1.71	−2.45	–	–	–	–

[a] All measured with a glassy carbon electrode. [b] Forward peak potential at 0.1 V.

that in the cobalt complexes is either cobalt centered or of a mixed metal-ligand nature.[32a,38] We attribute the differences in the potentials of the first reduction step to the operation of a similar phenomenon for the complexes described here. The effect of the PFC tail on the redox potentials of the complexes is marginal. On changing the solvent from CH_2Cl_2 to CH_3CN (Figure S2), additional redox steps are observed. The observance of additional reduction peaks at large cathodic potentials can be attributed to the larger solvent potential window of acetonitrile in comparison to dichloromethane (Tables 2 and S1). Additionally, some irreversible reduction peaks are observed, which are likely related to the dissociation of one or more of the tpy arms and the coordination of acetonitrile to the metal center. Even though the effect of the PFC tails on the redox potentials of the metal complexes is minimal, they do have a strong effect on the forms of the cyclic voltammetric responses. This effect is most prominent for complexes **5** and **6** that contain the longest PFC tail on the tpy ligands (Figure 5). A likely explanation is perhaps the movement of the PFC tails during redox processes, which would demand a large reorganization energy.

We also tried to investigate the UV-vis-NIR signatures of these metal complexes in the different redox states, and these data are provided in the Supporting Information. Unfortunately, the redox processes for most of the metal complexes were not reversible on the spectro-electrochemistry timescale. Hence no detailed discussion on the redox processes will be given here. Despite the irreversibility of the redox steps in the spectro-electrochemical timescale, the data are quantitatively similar to what was recently reported by us for related Fe^{II} and Co^{II} complexes.[32a] This aspect would also support the assignment of the redox steps, which was done above indirectly from electrochemical data.

EPR spectroscopy

For further investigations of the electronic structure, EPR spectra of the cobalt complexes **1**, **3** and **5** were measured. Spectra of all the complexes were recorded both, in the powder form as well as in acetonitrile solution.

Complex **1** displays an anisotropic EPR signal in frozen solution and in the solid state at 93 K, with partially resolved hyperfine splittings (Figure 6), which arises from interaction of the electron spin with the ^{59}Co nucleus ($I = {}^7/_2$). The simulation of the EPR spectra obtained from powdered samples of **1**, **3**
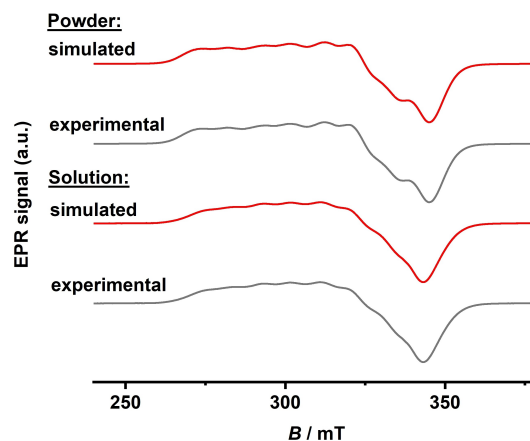
Figure 6. Experimental (gray) and simulated (red) EPR spectra of **1**, top: powdered sample at −180 °C; bottom: in acetonitrile at −180 °C.

and **5** were performed with rhombic **g** and **A** matrices (values given in Tables 3 and 4). In agreement with the Co—N distances determined from X-ray diffraction, the g values in the 2.00–2.20 range are consistent with a low-spin Co^{II} center. A metal-centered spin is clearly indicated for **1** by the rhombic **g** matrices, deviating from the free-electron value of 2, as well as the large hyperfine splitting. The unpaired electron would reside in the degenerate e_g orbitals in a perfectly octahedral geometry. This degeneracy is lifted by Jahn-Teller distortions, which might result in the unpaired electron being either on a $d_{x^2-y^2}$ or d_{z^2} orbital, or a mixture of the two, where the z-axis is that of the axial Jahn-Teller distortion.[39] It is indicated that

Table 3. Simulation parameters of **1** and **3**: g values, hyperfine A values [MHz], anisotropic Gaussian broadening HS [MHz] and isotropic Gaussian and Lorentzian broadenings [mT].

	1		3	
	Acetonitrile	Powder	Acetonitrile	Powder
g_x	2.003	2.008	2.075	2.087
g_y	2.152	2.172	2.075	2.017
g_z	2.202	2.189	2.219	2.267
A_x [MHz]	44	47	9	27
A_y [MHz]	93	94	10	~0
A_z [MHz]	283	287	194	132
HS_x [MHz]	2.38	0.24	–	–
HS_y [MHz]	90.57	121.3	–	–
HS_z [MHz]	187.36	175.4	–	–
line width for isotropic broadening [mT]	[1.8 2.6]	[0 2.0]	[15.5 0.5]	[12.1 4.3]

Chem. Eur. J. **2023**, *29*, e202301246 (7 of 15)

© 2023 The Authors. Chemistry - A European Journal published by Wiley-VCH GmbH

Chemistry–A European Journal

Research Article
doi.org/10.1002/chem.202301246

Chemistry Europe
European Chemical
Societies Publishing

Table 4. Simulation parameters of **5**: g values, hyperfine A values [MHz], anisotropic Gaussian broadening HS [MHz], axial A-strain and isotropic Gaussian and Lorentzian broadenings [mT].

	5 Acetonitrile/ PFO 1:2	Acetonitrile	Powder
g_x	2.056	2.085	2.048
g_y	2.091	2.085	2.107
g_z	2.199	2.170	2.182
A_x [MHz]	133	11.5	36
A_y [MHz]	29	~0	18
A_z [MHz]	293	158.3	136
HS_x [MHz]	104	–	–
HS_y [MHz]	32	–	–
HS_z [MHz]	0	–	–
AS_z [MHz]	40		
line width for isotropic broadening/mT	[1.0 2.0]	[8.3 2.2]	8.4

Figure 7. Experimental (gray) and simulated (red) EPR spectra of **3** top: powdered sample at −180 °C; bottom: in acetonitrile at −180 °C.

the magnetic orbital is an admixture of the $d_{x^2-y^2}$ or d_{z^2} orbitals due to the rhombic nature of the g values in complex **1**. For more than half-full d shells, if $g_z > g_x \sim g_y$, (usually called an axial spectrum even if there is a slight rhombicity) the unpaired electron is located in a $d_{x^2-y^2}$ orbital; on the other hand, if $g_z \sim 2.00 < g_x \sim g_y$ (usually called an inverted axial spectrum), the magnetic orbital is the d_{z^2}.[40] The latter is the most common case in low-spin Co^{II} complexes and most 3d^7 systems.[41] This is observed for **1**, indicating a mostly d_{z^2} magnetic orbital.

The spectra of **3** and **5** recorded in the solid state and in solution have similar g values while the A values differ (Tables 3 and 4). These differences are in accordance with small changes in the solution and solid-state structures, probably due to packing effects in the latter. The spectra in acetonitrile solution appear to be axial, suggesting a $d_{x^2-y^2}$ based SOMO, while in the powder samples the rhombicity is higher, which could be compatible with a d_{z^2} based SOMO with a certain degree of $d_{x^2-y^2}$ admixture. In all these cases the unresolved nature of the spectra limits the certainty with which the individual g values can be obtained. DFT calculations performed on a truncated version of complex **5** suggest a d_{z^2} ground state. These calculations will be discussed in the following section and in the Supporting Information.

For complexes **3** and **5**, no hyperfine splittings could be observed, and the spectra resembled those of exchange-narrowed extended magnetic systems (Figures 7 and 8).[30b,42] This phenomenon is suggestive of aggregation in solution, likely due to the F···F interactions of the PFC tails. To investigate this further, complexes **3** and **5** were measured in pentafluorobenzonitrile or a solution of acetonitrile/pentafluorobenzonitrile, respectively (Figure S24). For complex **5** additional measurements were performed in a mixture of 1:1 acetonitrile/1,2-difluorobenzene and in pure acetonitrile (Figure S25). As can be observed in the spectra, the diluted samples in acetonitrile, or in a mixture of acetonitrile and an aromatic fluorinated solvent, show a partially resolved hyperfine structure. This suggests that aggregation is partially
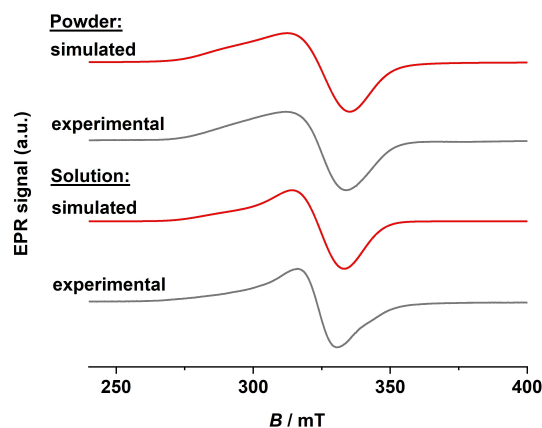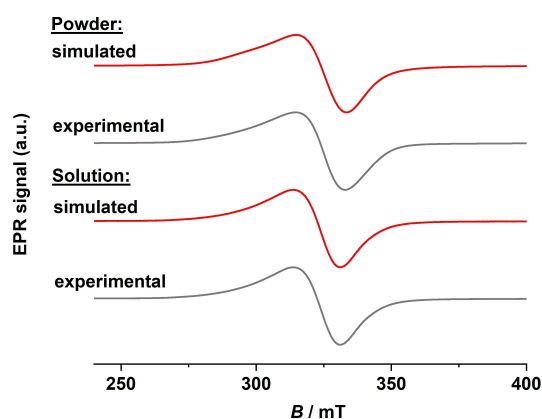
Figure 8. Experimental (gray) and simulated (red) EPR spectra of **5** left: powdered sample at −180 °C; right: in acetonitrile at −180 °C.

avoided in these conditions, and further supports the association of the aggregation effect with the exchange-narrowed characteristics of the spectra. Finally, the measurements were performed with different ratios of an acetonitrile/perfluorooctanol (PFO) solution. Already with 1% of PFO a disruption of the complex aggregates is apparent and at a 3:1 (acetonitrile/PFO) ratio hyperfine splitting is observed for both investigated complexes, which leads to the assumption that the fluorine-specific interactions between the complexes are inhibited (Figure 9). For higher ratios of PFO only marginal changes in the spectra can be observed. Comparing these results to complex **1** where no exchange narrowing was observed, the fluorine-specific interactions of the PFC tails seem to have a huge impact on the aggregation of the molecules, thus leading to the observed exchange narrowing. To the best of our knowledge, this is the first time that aggregation-mediated exchange narrowing has been observed with reference to fluorine-specific interactions of fluorinated alkyl chains.
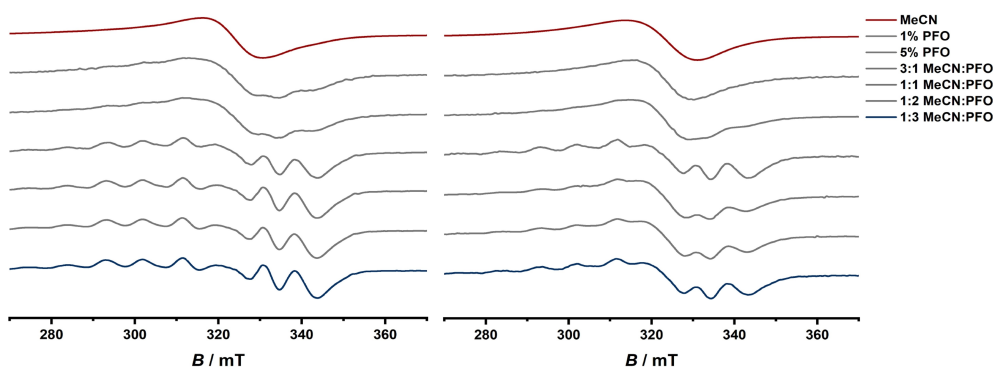
Chemistry–A European Journal

Research Article
doi.org/10.1002/chem.202301246

Chemistry Europe
European Chemical
Societies Publishing

Figure 9. EPR measurements of **3** (left) and **5** (right) with different ratios of acetonitrile/PFO.

Density functional theory calculations

DFT calculations, performed using the ORCA program (version 5.0),[43] were applied to a truncated form of complex **5** (see the Supporting Information for further details). In order to calculate the exchange coupling between neighbouring molecules of complex **5**, two different truncated forms of the complex where designed based on the crystal structure of **5**. In one case, **5**$_{tr1}$ (Figures S26 and S27), the fluorinated portion of the fluoroalkane chain was removed, leaving only the first $-CF_2$ group, which was capped with another F atom, following approximately the same bond distances and angles as the capping $-CF_3$ in the original complex. The monomer **5**$_{tr1}$ was separately optimized (TPSSh/def2-SVP) in order to obtain the energies and orbitals around the SOMO-LUMO gap and determine the occupation of the 3d orbitals (Figure S26). For the dimer composed of two nonoptimized **5**$_{tr1}$ complexes, the BF_4^- counter ions were maintained, and the molecular cluster had a net charge of zero. The following truncated form, **5**$_{tr2}$ (Figure S28), was terminated with a $-OCH_3$ group, and in this calculation the counter ions were removed, giving a system with $+4$ charge. For the calculation of exchange interactions between neighbours, the geometries were not optimized, as the purpose was to estimate the exchange coupling in the crystal, and the truncation of the long fluoroalkyl chains would have undoubtedly perturbed the packing considerably. As we believed the exchange coupling to be transmitted through weak π-π interactions, which are very sensitive to the distance and the eclipsed area between aromatic fragments, any small change in structure would have large effects in the exchange coupling, and we considered the unperturbed crystal structure to be the safest model. The calculation of $[\mathbf{5}_{tr1}]^{2+}$ revealed that the unpaired electron resides in a $3d_{z^2}$ orbital (Figure S26), as do the spin densities for the broken symmetry calculations (Figures S27 and S28), although with a certain degree of admixture with the $3d_{x^2-y^2}$ orbital. Calculated **g** matrices using TPSSh (10% HF exchange) or TPSS0 (25% HF exchange) functionals (Figure S29 and Table S4) reveal highly rhombic **g** matrices, although with smaller *g* deviations from the free electron *g* value, which is a known limitation of DFT methods in the case of anisotropic transition metal complexes. The

calculations predict that the smallest *g* value is roughly in the direction of the $3d_{z^2}$ orbital, while the highest is roughly directed along the shortest Co–N distances, corresponding to the central pyridine composing the ligand. An in-depth analysis of the EPR properties of Co^{II} terpyridine complexes, containing long alkyl chains, was performed by Murray et al.[39a] The authors were able to simulate EPR spectra in solution quite similar to the one shown in Figures 9 and 10 with a very rhombic **g** matrix and **A** matrix, and concluded that the lowest *g* value was associated with the direction of tetragonal elongation in the complex, and compatible with a $3d_{z^2}$ magnetic orbital aligned with the elongated axis, in agreement with our DFT results. While Murray et al. in general found resolved hyperfine splittings in solution, we observed for **3** and **5** exchange narrowed spectra, and needed to add fluorinated solvents to observe partially or totally resolved hyperfine splittings. In order to estimate the very small exchange couplings, presumably mediated by π-π interactions, that could lead to the exchange narrowing in solution, we had to perform calculations with a good theory level, tight convergence settings and accurate integration grids. Table S1 shows the results of Broken Symmetry calculations performed with Orca on the $[\mathbf{5}_{tr1}(BF_4)_2]_2$ and $[\mathbf{5}_{tr2}]_2^{4+}$ models, using the
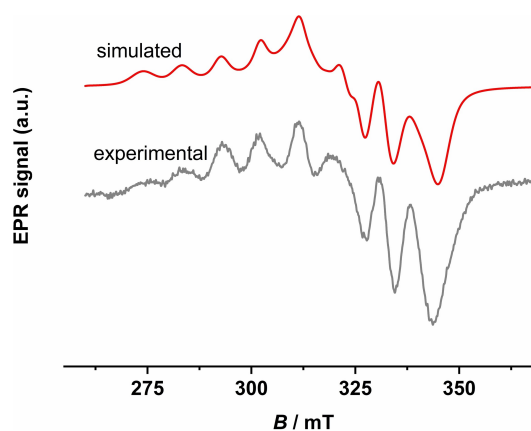

Figure 10. EPR measurement of **5** in a 1:2 acetonitrile/PFO mixture, together with the corresponding simulation (Table 4).

Chemistry–A European Journal

Research Article
doi.org/10.1002/chem.202301246

Chemistry Europe
European Chemical
Societies Publishing

hybrid meta-GGA functional, TPSSh, with def2-TZVP basis sets on all atoms. Calculations were performed using TightSCF and DefGrid3 options in Orca. The calculated exchange coupling constants are both ferromagnetic, with values of 0.17 and 0.10 cm^{-1}, respectively, which amount to ~180 and ~107 mT. These values should be considered approximate, since they correspond to very small energy differences between the high-spin and broken symmetry states, on the order of 10^{-6}–10^{-7} Ha. Furthermore, even if the values are accurately calculated for the crystal, there are no guarantees that the same values are obtained for aggregated molecules in solution. However, the small values of the exchange constants are one order of magnitude larger than the hyperfine splitting of complex **5** in an MeCN/PFO mixture, and therefore appear to be enough to cause exchange narrowing of the EPR signals of the complex when this is aggregated in pure MeCN. The magnitude of the exchange coupling (~0.1–0.2 cm^{-1}) transmitted through π-π interactions between the terpyridine ligands, is much smaller than the values found for systems where the magnetic centers are connected through extended covalent pathways, and even small compared to exchange couplings transmitted through pathways involving H-bonds.[30b] These values are too small to be observed by standard magnetic measurements, and are usually only revealed by EPR spectroscopy, which is especially suitable to observe very small magnetic interactions. It has been shown before that π-π interactions are able to transmit very weak exchange interactions between magnetic metal centers ligated by polypyridyl[44] and phenanthrolyl ligands.[31b,42b] As summary, we have observed the exchange narrowing effect in solution, which happens for the Co^{II} bis-terpyridine complexes with long fluoroalkyl chains and not for the −OCF$_3$ substituted one, nor the alkane substituted complexes reported by Murray et al., and therefore is highly suggestive of aggregation induced by F···F interactions. The exchange narrowing phenomenon is caused by very small exchange interactions between neighboring Co^{II} centers communicated by non-covalent, π-π interactions.

Conclusion

We have successfully synthesized terpyridine ligands with different PFC tails and the corresponding homoleptic Co^{II} and Fe^{II} complexes. The cyclic voltammograms show marginal differences in the redox potentials upon changing the substituents in the ligand backbone. However, changing the metal centers as well as using different solvents leads to different redox potentials and additional processes. This is probably due to the coordination of acetonitrile molecules during the measurement. For complexes **1**, **2** and **5** we were able to obtain solid-state structures that showed the intermolecular interactions in the crystal packing. The bond distances of the complexes indicate a LS center at 100 K. The SCO behavior of the complexes was investigated through SQUID magnetometric measurements. Complex **1** does not exhibit SCO behavior, but the measurements indicate that the

measured sample contains Co^{II} molecules in the HS as well as the LS state. The Co^{II} centers in complexes **3** and **5** display an incomplete SCO, while the Fe^{II} complexes remain in the LS state over the measured temperature range. This is also supported by ^{1}H NMR spectroscopy, which indicates a Fe^{II} LS center at room temperature. The magnetic properties of the cobalt complexes are influenced by the length of the PFC tails.

To further determine the fluorine-specific interactions, several EPR experiments were performed. An exchange narrowing was observed during the measurement of complexes **3** and **5** as powdered samples, as well as in frozen acetonitrile solution. By adding different amounts of PFO, the aggregation of the complexes could be disrupted, as confirmed from by hyperfine coupling. To the best of our knowledge, this is the first time that fluorine-specific interactions of the PFC tails and the influence thereof on exchange narrowing have been investigated by EPR measurements.

Experimental Section

Compounds: Ligands **2** and **3** were synthesized following published procedures.[4] Commercially available chemicals were used without further purification. Dry solvents were available from MBRAUN MB-SPS-800 solvent system. All solvents were degassed by standard techniques prior to use. Column chromatography was conducted using aluminium oxide (aluminium oxide basic, Macherey-Nagel, 50–200 μm). ^{1}H NMR, proton decoupled ^{13}C and ^{19}F NMR were recorded on JEOL ECS 400 spectrometer and JEOL ECZ 400R spectrometer at 20 °C. Chemical shifts are reported in ppm (relative to the TMS signal) with reference to the residual solvent peaks.[45] Multiplets are reported as follows: singlet (s), doublet (d), triplet (t), quartet (q), quintet (quint), septet (sept), and combinations thereof. Mass spectrometry was performed on an Agilent 6210 ESI-TOF. Elemental analysis was performed on a Perkin Elmer Analyser 240.

Electrochemistry: Cyclic voltammograms were recorded with a PAR VersaStat 4 potentiostat (Ametek) by working in anhydrous and degassed acetonitrile or dichloromethane with 0.1 M NBu$_4$PF$_6$ (dried, >99.0%, electrochemical grade, Fluka) as supporting electrolyte. Concentrations of the complexes were about $1 \cdot 10^{-4}$ M. A three-electrode setup was used with a glassy carbon working electrode, a coiled platinum wire as counter electrode, and a coiled silver wire as a pseudoreference electrode. The ferrocene/ferrocenium or decamethylferrocene/decamethylferrocenium couples were used as internal reference.

UV/Vis spectra were recorded with an Avantes spectrometer consisting of a light source (AvaLight-DH-S-Bal), a UV/VIS detector (AcaSpec-ULS2048), and an NIR detector (AvaSpec-NIR256-TEC). Spectro-electrochemical measurements were carried out in an optically transparent thin-layer electrochemical (OTTLE) cell (CaF2 windows) with a gold working electrode, a platinum mesh counter electrode, and a silver-foil pseudoreference electrode.[46] Anhydrous and degassed acetonitrile or dichloromethane with 0.1 M NBu$_4$PF$_6$ as supporting electrolyte was used as solvent.

Electron paramagnetic resonance: EPR spectra at X-band frequency (ca. 9.5 GHz) were obtained with a Magnettech MS-5000 benchtop EPR spectrometer equipped with a rectangular TE 102 cavity and TC HO4 temperature controller. The measurements were carried out in synthetic quartz glass tubes.

X-ray diffraction: X-ray data were collected on a Bruker Smart AXS or Bruker D8 Venture system at 100(2) K, respectively, using

Chemistry–A European Journal

Research Article
doi.org/10.1002/chem.202301246

Chemistry Europe
European Chemical
Societies Publishing

graphite-monochromated Moα radiation ($\lambda\alpha = 0.71073$ Å). Using the Smart software or using the APEX2 software, respectively, evaluated the strategy for the data collection. The data were collected by the standard omega scan or omega+phi scan techniques, and were scaled and reduced using Saint+ and SADABS software. Direct methods or intrinsic phasing using SHELXT-2014/7 solved the structures. Structures were refined by full matrix least-squares using SHELXL-2014/7, refining on $F2$. Non-hydrogen atoms were refined 40 anisotropically.[47] Deposition Number 2201104 (for **1**), 2201105 (for **2**), and 2201107 (for **5**) contains the supplementary crystallographic data for this paper. These data are provided free of charge by the joint Cambridge Crystallographic Data Centre and Fachinformationszentrum Karls-ruhe Access Structures service.

SQUID magnetometry: All susceptibility measurements were carried out on a Quantum Design MPMS3 SQUID magnetometer. The measurements at a constant magnetic field of 1000 Oe in a temperature range from 1.8 to 50 K and at 10 000 Oe in a temperature range from 40 to 300 K. The measured data in the intersection of the temperature ranges served to compensate for possible ferromagnetic impurities. Samples were pounded with little pressure and mixed with eicosane. The mixture was melted in a capsule with a hot air gun maximized to a temperature of 50 °C (323.15 K) and the capsule was then fixed in a plastic tube. The temperature dependent measurements were limited to a temperature of 300 K due to the melting of the used eicosane matrix (melting point of eicosane: 311 K). Data were corrected for the diamagnetic contribution to the susceptibility by means of Pascal's constants.[48]

DFT calculations: All calculations were performed using the ORCA program.[43] Geometry optimizations were carried out using the TPSSh functional[49] with def2-SVP basis sets[50] on all atoms, starting from the X-ray determined structures. The optimized structures were used for single point and frequency calculations with the TPSSh functional and def2-TZVP basis sets. A particular calculation of the g and A matrices was also performed using the TPSS0 functional[51] (with 25% HFx) and a def2-QZVP basis set on the Co atom. The resolution-of-the-identity (RI) approximation[52] with matching basis sets (def2/J),[53] as well as the RIJCOSX approximation (combination of RI and chain-of-spheres algorithm for exchange integrals) were used to reduce the time of calculations. The optimized structures were confirmed to be minima by the absence of imaginary vibrational frequencies. Orbital and electron density isosurfaces were plot with Chemcraft. (Chemcraft–graphical software for visualization of quantum chemistry computations. http://www.chemcraftprog.com).

Synthesis: 3,3,4,4,5,5,6,6,7,7,8,8,8-Tridecafluorooctyl trifluorometha-nesulfonate and 3,3,4,4,5,5,6,6,7,7,8,8,9,9,10,10,10-heptadecafluoro-decyl trifluoromethanesulfonate were synthesized according to literature known procedures.[54]
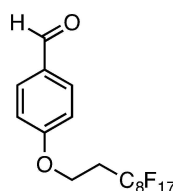
Benzaldehyde R$_f$Oct
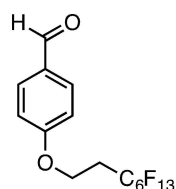
The synthesis was performed according to a literature known procedure.[4] 4-Hydroxy benzaldehyde (500 mg, 4.09 mmol, 1.0 equiv.) was placed in a 100 mL round bottom flask and
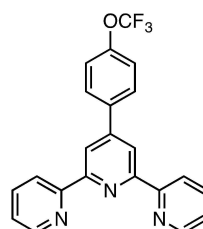
dissolved in acetone (60 mL). Then, K$_2$CO$_3$ (1.13 g, 8.18 mmol, 2.0 equiv.) and 18-crown-6 (541 mg, 2.05 mmol, 0.5 equiv.) were added and the suspension was stirred at RT for 30 min. Afterwards, the alkyl triflate (2.44 g, 4.91 mmol, 1.2 equiv.) was added and the reaction mixture was refluxed for additional 48 h. The precipitate was filtered off, the solvent was removed and the crude product was purified by column chromatography (SiO$_2$, n-pentane→n-pentane/EtOAc 5:1), affording the product (1.10 g, 2.3 mmol, 57%) as a colorless solid. ^{1}H NMR (401 MHz, CDCl$_3$): $\delta = 9.91$ (s, 1H), 7.86 (d, $J = 8.8$ Hz, 2H), 7.02 (d, $J = 8.7$ Hz, 2H), 4.36 (t, $J = 6.7$ Hz, 2H), 2.68 (tt, $J = 18.2$, 6.7 Hz, 2H) ppm. ^{19}F NMR (377 MHz, CDCl$_3$): $\delta = $-80.6 (tt, $J = 10.0$, 2.4 Hz), -113.1–(-133.3) (m), -121.5–(-122.0) (m), -122.7–(-122.8) (m), -123.4–(-123.4) (m), -126.0–(-126.1) (m) ppm. ^{13}C NMR (151 MHz, CDCl$_3$): $\delta = 190.9$, 163.1, 132.2, 130.7, 114.9, 60.5, 31.3 (t, $J = 21.7$ Hz) ppm. The signals of the fluorinated carbon atoms are missing due to poor signal-to-noise ratio. HRMS (ESI): calcd. for $[C_{15}H_9F_{13}O_2Na]^+$ $[M-Na]^+$: m/z 491.0287; found 491.0361. Anal. calcd. for $C_{15}H_9F_{13}O_2 \cdot 0.1\,C_5H_{12}$: C 39.16, H 2.16, N 0; found: C 39.02, H 1.98, N 0.03.

Benzaldehyde R$_f$Dec
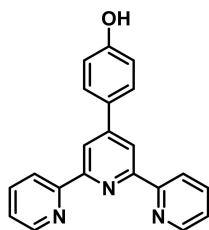

The synthesis was performed according to a literature known procedure.[4] 4-Hydroxy benzaldehyde (122 mg, 1.00 mmol, 1.0 equiv.) was placed in a 50 mL round bottom flask and dissolved in acetone (15 mL). Then, K$_2$CO$_3$ (276 mg, 2.00 mmol, 2.0 equiv.) and 18-crown-6 (132 mg, 500 µmol, 0.5 equiv.) were added and the suspension was stirred at RT for 30 min. Afterwards, the alkyl triflate (894 mg, 1.50 mmol, 1.5 equiv.) was added and the reaction mixture was refluxed for additional 48 h. The precipitate was filtered off, the solvent was removed and the crude product was purified by column chromatography (SiO$_2$, n-pentane→n-pentane/EtOAc 5:1), affording the product (399 mg, 0.7 mmol, 70%) as a colorless solid. ^{1}H NMR (401 MHz, CDCl$_3$): $\delta = 9.91$ (s, 1H), 7.86 (d, $J = 8.6$ Hz, 2H), 7.02 (d, $J = 8.6$ Hz, 2H), 4.36 (t, $J = 6.7$ Hz, 2H), 2.68 (tt, $J = 18.1$, 6.6 Hz, 2H) ppm. ^{19}F NMR (377 MHz, CDCl$_3$): $\delta = $-80.6 (t, $J = 9.9$ Hz), -113.2 (p, $J = 17.7$ Hz), -121.3–(-121.6) (m,), -121.6–(-121.9) (m), -122.5–(-122.9) (m), -123.2–(-123.4) (m), -125.8–(-126.1) (m) ppm. ^{13}C NMR (151 MHz, CDCl$_3$): $\delta = 190.9$, 163.1, 132.2, 130.7, 114.9, 60.5, 31.4 ppm. The signals of the fluorinated carbon atoms are missing due to poor signal-to-noise ratio. HRMS (ESI): calcd. for $[C_{15}H_9F_{17}O_2Na]^+$ $[M-Na]^+$: m/z 591.0223; found 591.0231. Anal. calcd. for $C_{17}H_9F_{17}O_2 \cdot 0.1\,C_5H_{12} \cdot 0.25\,CH_2Cl_2$: C 35.73, H 1.81, N 0; found: C 36.11, H 2.19, N 0.03.

TPYPhOCF$_3$L1

Chemistry–A European Journal

Research Article
doi.org/10.1002/chem.202301246

**Chemistry Europe**
European Chemical
Societies Publishing

The synthesis was performed according to a literature known procedure.[33] 4-Trifluoromethoxy benzaldehyde (0.90 mL, 6.3 mmol, 1.0 equiv.) was placed in a 50 mL round bottom flask and dissolved in EtOH/H$_2$O (2:1, 15 mL). 2-Acetylpyridine (1.4 mL, 12.6 mmol, 2.0 equiv.), NH$_3$ (aq. solution, 25 wt.%, 20 mL) and NaOH (957 mg, 23.9 mmol, 3.8 equiv.) were added and the solution was stirred at RT for 48 h. The formed viscous residue was filtered off, dissolved in a minimal amount of EtOH, and the crude product was precipitated by slowly adding water to the solution. The solid was filtered off and washed with a mixture of EtOH/H$_2$O (1:1, 5×20 mL) to afford the product (1.20 g, 3.0 mmol 48%) as a pale yellow solid. ^{1}H NMR (600 MHz, CDCl$_3$): $\delta = 8.73$ (d, $J = 4.4$ Hz, 2H), 8.71 (s, 2H), 8.67 (d, $J = 7.9$ Hz, 2H), 7.92 (d, $J = 8.6$ Hz, 2H), 7.88 (td, $J = 7.7, 1.7$ Hz, 2H), 7.38-7.33 (m, 4H) ppm. ^{19}F NMR (565 MHz, CDCl$_3$): $\delta = -57.6$ ppm. ^{13}C NMR (151 MHz, CDCl$_3$): $\delta = 156.3, 156.2, 150.0, 149.3, 149.1, 137.4, 137.1, 129.0, 124.1, 121.5, 121.4, 119.8, 118.9$ ppm. HRMS (ESI): calcd. for [C$_{22}$H$_{15}$F$_3$N$_3$O]$^+$: m/z 394.1162; found 394.1148. Anal. calcd. for C$_{22}$H$_{14}$F$_3$N$_3$O: C 67.17, H 3.59, N 10.68; found: C 67.29, H 3.63, N 10.79.

TPYPhOH

The synthesis was performed according to a literature known procedure.[33] 4-Hydroxybenzaldehyde (1.2 g, 10 mmol) was dissolved in 15 mL EtOH/H$_2$O (2:1) and 2-acetylpyridine (2.4 g, 20 mmol) was added, followed by NaOH (1.5 g, 26 mmol) and 30 mL of ammonia solution (25%). The mixture was stirred at room temperature overnight, the white precipitate was filtered and washed with water (5×10 mL) and ethanol (3×5 mL) yielding a white solid (920.5 mg, 2.8 mmol, 28%). ^{1}H NMR (DMSO, 401 MHz, 21°C): $\delta = 8.74$ (d, $J = 5.0$ Hz, 2H), 8.62 (d, $J = 7.9$ Hz, 2H), 8.55 (s, 2H), 7.99 (td, $J = 7.8, 2.2$ Hz, 2H), 7.66–7.27 (m, 4H), 6.39 (d, $J = 8.7$ Hz, 2H) ppm.
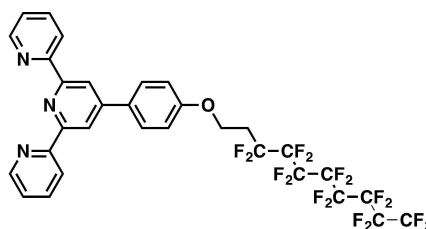
TPYPhRfOct L2
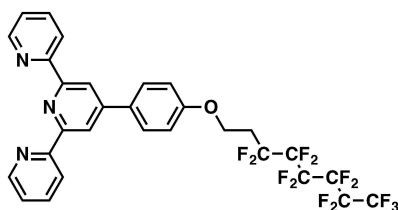
Route 1: The synthesis was performed according to a literature known procedure.[4] TPYPhOH (650.7 mg, 2.0 mmol), K$_2$CO$_3$ (420.0 mg, 3.0 mmol) and 18-crown-6 (264.0 mg, 1.0 mmol) were dissolved in acetone (45 mL) and stirred at room temperature for one hour. Afterwards R$_f$Oct-OTf (1.5 g, 4 mmol) was added and the mixture was stirred at 60°C overnight. After cooling to room temperature the white precipitate was filtered and the solvent was removed under reduced pressure. The crude product was purified by column chromatography (basic Al$_2$O$_3$, DCM) yielding in a yellow solid (86.6 mg, 0.1 mmol, 6%).
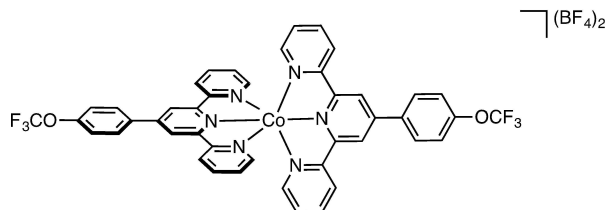
Route 2: 2-Acetylpyridine (0.50 mL, 4.44 mmol, 2.0 equiv.) and TPYPhR$_f$Oct (1.04 g, 2.22 mmol, 1.0 equiv.) were placed in a 50 mL round bottom flask and dissolved in EtOH/H$_2$O (2:1, 12 mL). Then, NH$_3$ (aq. solution, 25 wt.%, 6 mL) and NaOH (340 mg, 8.50 mol, 3.8 equiv.) were added and the solution was stirred for 48 h at 60°C. The formed precipitate was filtered off and washed with water (3×15 mL) and EtOH (3×15 mL), affording the product (350 mg, 1.0 mmol, 23%) as a colorless solid. ^{1}H NMR (CDCl$_3$, 400 MHz, 20°C): $\delta = 8.80$–8.72 (m, 2H), 8.71 (s, 2H), 8.67 (dt, $J = 8.0, 1.0$ Hz, 2H), 7.35 (ddd, $J = 7.4, 4.8, 1.2$ Hz, 4H), 7.07–7.01 (m, 2H), 4.36 (t, $J = 6.9$ Hz, 2H), 2.68 (ddd, $J = 24.8, 18.2, 6.7$ Hz, 2H) ppm. ^{13}C NMR (CDCl$_3$, 101 MHz, 0°C): $\delta = 159.1, 157.3, 150.6, 149.3, 137.8, 128.8, 123.9, 122.0, 119.6, 115.7$ ppm. ^{19}F NMR (CDCl3, 376 MHz, 0°C): $\delta = -80.6, -113.11$ (q, $J = 17.3, 15.5$ Hz), $-121.7, -122.7, -123.4, -125.99$ (dq, $J = 13.8, 6.9$ Hz) ppm. HRMS (ESI): calcd. For [C$_{29}$H$_{18}$F$_{13}$N$_3$ONa]$^+$: m/z 694.1134; found 694.1106. Anal. Calcd for C$_{29}$H$_{18}$F$_{13}$N$_3$O·0.1 C$_5$H$_{12}$: C 52.21, H 2.85, N 6.19; found: C 52.04, H 3.15, N 6.26.

TPYPhRfDec L3

Route 1: The synthesis was performed according to a literature known procedure.[4] TPYPhOH (325.4 mg, 1.0 mmol), K$_2$CO$_3$ (210.0 mg, 1.5 mmol) and 18-crown-6 (132.0 mg, 0.5 mmol) were dissolved in acetone and stirred at room temperature for one hour. Afterwards R$_f$Dec-OTf (1.2 g, 2 mmol) was added and the mixture was stirred at 60°C overnight. After cooling to room temperature the white precipitate was filtered and the solvent was removed under reduced pressure. The crude product was purified by column chromatography (basic Al$_2$O$_3$, DCM) yielding in a yellow solid (127.5 mg, 0.16 mmol, 16%).

Route 2: 2-Acetylpyridine (0.40 mL, 3.56 mmol, 2.0 equiv.) and TPYPhR$_f$Dec (1.01 g, 1.78 mmol, 1.0 equiv.) were placed in a 50 mL round bottom flask and dissolved in EtOH/H$_2$O (2:1, 12 mL). Then, NH$_3$ (aq. solution, 25%, 6 mL) and NaOH (270 mg, 6.75 mol, 3.8 equiv.) were added and the solution was stirred for 24 h at 60°C. The formed precipitate was filtered off and washed with water (3×15 mL) and EtOH (3×15 mL), affording the product (187 mg, 0.57 mmol, 16%) as a pale yellow solid. ^{1}H NMR (CDCl$_3$, 400 MHz, 20°C): $\delta = 8.73$ (d, $J = 4.8$ Hz, 0H), 8.70 (s, 2H), 8.67 (d, $J = 7.9$ Hz, 2H), 7.93–7.84 (m, 4H), 7.36 (dd, $J = 6.9, 5.4$ Hz, 2H), 7.03 (d, $J = 8.7$ Hz, 2H), 4.35 (t, $J = 6.8$ Hz, 2H), 2.68 (ddd, $J = 25.1, 18.2, 6.7$ Hz, 2H) ppm. ^{13}C NMR (CDCl$_3$, 101 MHz, 20°C): $\delta = 159.1, 156.4, 156.0, 149.3, 137.1, 128.9, 124.0, 121.6, 118.5, 115.9$ ppm. ^{19}F NMR (CDCl$_3$, 377 MHz, 21°C): $\delta = -80.84$ (s), -113.35–-113.73 (m), -121.87 (d, $J = 83.8$ Hz), -122.89 (d, $J = 82.7$ Hz), -123.64 (d, $J = 84.2$ Hz), -126.19 ppm. HRMS (ESI): calcd. For [C$_{31}$H$_{19}$F$_{17}$N$_3$O]$^+$; m/z 772.1251; found 772.1212. Anal. Calcd for C$_{31}$H$_{18}$F$_{17}$N$_3$O·1.3 H$_2$O: C 46.84, H 2.61, N 5.29; found: C 46.54, H 2.28, N 5.45.

Chemistry–A European Journal

Research Article
doi.org/10.1002/chem.202301246

Chemistry Europe
European Chemical
Societies Publishing

[Co(TpyPhOCF₃)₂](BF₄)₂ 1

Co(BF₄)₂·6 H₂O (17.0 mg, 0.05 mmol) was dissolved in 10 mL methanol and TPYPhOCF₃ (39.3 mg, 0.10 mmol) was added. The mixture was stirred for four days. The solvent was evaporated and the product was purified by crystallization in MeCN/Et₂O yielding in dark orange crystals (32.0 mg, 0.03 mmol, 62 %). HRMS (ESI): calcd. for $[C_{44}H_{28}CoF_6N_6O_2]^{2+}$ $[M-(BF_4)_2]^{2+}$: m/z 422.5749; found 422.5780. Anal. calcd. for $C_{44}H_{28}B_2CoF_{14}N_6O_2 \cdot 0.5\,C_2H_3N \cdot 0.25\,C_4H_{10}O$: C 52.21, H 3.05, N 8.60; found: C 52.11, H 3.12, N 8.67.

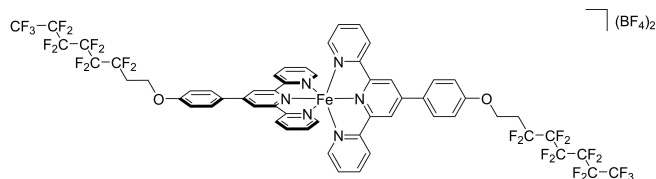## [Fe(TpyPhOCF₃)₂](BF₄)₂ 2
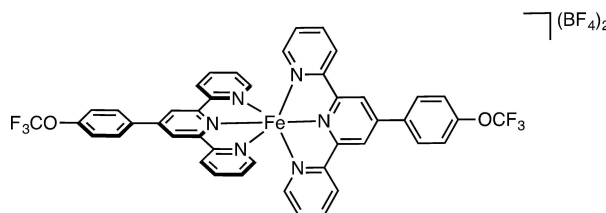
Fe(BF₄)₂·6 H₂O (16.8 mg, 0.05 mmol) was dissolved in 10 mL methanol and TPYPhOCF₃ (39.3 mg, 0.10 mmol) was added. The mixture was stirred for four days. The solvent was evaporated and the product was purified by crystallization in MeCN/Et₂O yielding in dark violet crystals. (36.0 mg, 0.03 mmol, 73 %). ^{1}H NMR (600 MHz, CD₃CN): $\delta = 9.19$ (s, 4H), 8.62 (d, $J = 7.9$ Hz, 4H), 8.42 (d, $J = 8.6$ Hz, 4H), 7.92 (t, $J = 7.3$ Hz, 4H), 7.74 (d, $J = 8.2$ Hz, 4H), 7.20 (d, $J = 5.4$ Hz, 4H), 7.10 (t, $J = 6.4$ Hz, 4H) ppm. ^{19}F NMR (377 MHz, CD₃CN): $\delta = -58.3, -151.5, -151.5$ ppm. ^{13}C NMR (151 MHz, CD₃CN): $\delta = 161.4$, 159.0, 154.1, 151.7, 150.0, 139.8, 136.9, 131.0, 128.4, 125.0, 123.1, 122.8, 122.5, 120.8 ppm. One more signal than expected is observed. This might be due to poor signal-to-noise ratio, so that no full resolution of the quartet expected for C–F coupling is possible. HRMS (ESI): calcd. for $[C_{44}H_{28}F_6FeN_6O_2]^{2+}$ $[M-(BF_4)_2]^{2+}$: m/z 421.0758; found 421.0826. Anal. calcd. for $C_{44}H_{28}F_6FeN_6O_2$: C 52.01, H 2.78, N 8.27; found: C 52.06, H 2.99, N 8.40.

[Co(TpyPhORfOct)₂](BF₄)₂ 3
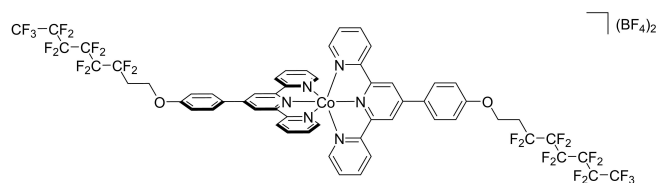
Co(BF₄)₂·6 H₂O (20.57 mg, 0.06 mmol) was dissolved in 10 mL methanol and 4′-(4-((3,3,4,4,5,5,6,6,6-nonafluorohexyl)oxy)phenyl)-2,2′:6′,2′′-terpyridine (81.10 mg, 0.12 mmol) was added. The mixture was stirred for one week, the solvent was evaporated and the crude product was dissolved in acetonitrile and precipitated in EtOH, yielding in a red solid (16.4 mg, 0.01 mmol, 17 %). HRMS (ESI): calcd. For $[C_{58}H_{36}CoF_{26}N_6O_2]^{2+}$ $[M-(BF_4)_2]^{2+}$: m/z 700.5903; found

700.5934. $C_{58}H_{36}B_2CoF_{34}N_6O_2 \cdot 1.2\,C_2H_3N \cdot 1.75\,H_2O \cdot 0.4\,CH_2Cl_2$: C 43.21, H 2.62, N 5.97; found: C 43.09, H 2.49, N 6.08.

[Fe(TpyPhORfOct)₂](BF₄)₂ 4

Fe(BF₄)₂·6 H₂O (17.12 mg, 0.05 mmol) was dissolved in 10 mL methanol and 4′-(4-((3,3,4,4,5,5,6,6,6-nonafluorohexyl)oxy)phenyl)-2,2′:6′,2′′-terpyridine (68,10 mg, 0.01 mmol) was added. The mixture was stirred for four days, the solvent was evaporated and the crude product was dissolved in acetonitrile and precipitated in EtOH, yielding in a red solid (30.90 mg, 0.02 mmol, 39 %). ^{1}H NMR (500 MHz, CD₃CN): $\delta = 9.15$ (s, 4H), 8.61 (s, 4H), 8.32 (s, 3H), 7.91 (s, 4H), 7.37 (s, 3H), 7.19 (s, 5H), 7.09 (s, 5H), 4.54 (s, 4H), 2.84 (m, 4H) ppm. ^{19}F NMR (471 MHz, CD₃CN): $\delta = -81.4, -113.4, -122.1, -123.2, -123.9, -126.4, -151.4$ ppm. ^{13}C NMR (151 MHz, CD₃CN): $\delta = 161.4$, 161.1, 159.0, 153.9, 150.7, 139.5, 130.3, 128.1, 124.6, 121.8, 116.6, 61.5, 31.6 (t, $J = 21.3$ Hz) ppm. HRMS (ESI): calcd. For $[C_{58}H_{36}F_{26}FeN_6O_2]^{2+}$ $[M-(BF_4)_2]^{2+}$: m/z 699.0912; found 699.0909. Anal. Calcd for $C_{58}H_{36}B_2F_{34}FeN_6O_2 \cdot 2.3\,C_2H_3N \cdot 1\,C_4H_{10}O$: C 45.95, H 3.06, N 6.68; found: C 46.33, H 2.67, N 6.29.

[Co(TpyPhORfDec)₂](BF₄)₂ 5
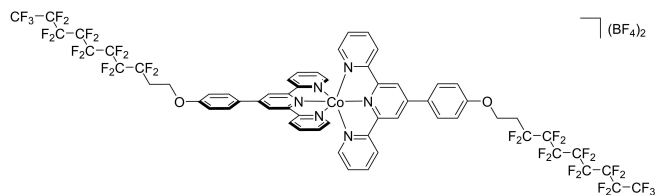
Co(BF₄)₂·6 H₂O (12.20 mg, 0.04 mmol) was dissolved in 10 mL methanol and 4′-(4-((3,3,4,4,5,5,6,6,7,7,8,8,8-tridecafluorooctyl)oxy)phenyl)-2,2′:6′,2′′-terpyridine (74.60 mg, 0.07 mmol) was added. The mixture was stirred for two days, the solvent was evaporated and the crude product was dissolved in acetonitrile and precipitated in EtOH, yielding in a red solid (35.20 mg, 0.02 mmol, 55 %). Crystals suitable for X-ray diffraction were grown by slow evaporation of an acetonitrile solution of the complex. HRMS (ESI): calcd. For $[C_{62}H_{36}CoF_{34}N_6O]^{2+}$ $[M-(BF_4)_2]^{2+}$: m/z 800.5839; found 800.5877. Anal. Calcd for $C_{62}H_{36}B_2F_{42}CoN_6O_2$: C 41.94, H 2.04, N 4.73; found: C 41.95, H 2.12, N 4.84.

[Fe(TpyPhORfDec)₂](BF₄)₂ 6
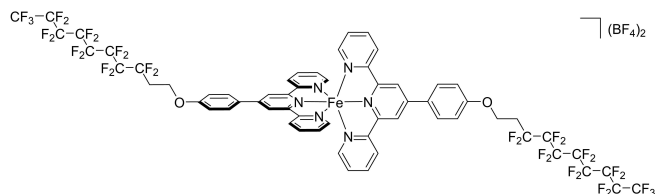
Fe(BF₄)₂·6 H₂O (18.37 mg, 0.05 mmol) was dissolved in 10 mL methanol and 4′-(4-((3,3,4,4,5,5,6,6,7,7,8,8,8-tridecafluorooctyl)oxy)phenyl)-2,2′:6′,2′′-terpyridine (84.00 mg, 0.11 mmol) was added. The mixture was stirred for one week, the

Chemistry–A European Journal

Research Article
doi.org/10.1002/chem.202301246

Chemistry Europe
European Chemical
Societies Publishing

solvent was evaporated and the crude product was dissolved in acetonitrile and precipitated in EtOH, yielding in a purple solid (50.60 mg, 0.03 mmol, 57%). ^{1}H NMR (401 MHz, CD$_3$CN): $\delta = 9.14$ (s, 3H), 8.60 (d, $J = 8.4$ Hz, 4H), 8.31 (d, $J = 8.4$ Hz, 3H), 7.94–7.86 (m, 5H), 7.36 (d, $J = 8.7$ Hz, 3H), 7.18 (d, $J = 6.1$ Hz, 5H), 7.07 (t, $J = 5.8$ Hz, 5H), 4.54 (t, $J = 6.0$ Hz, 2H), 3.75 (t, $J = 6.1$ Hz, 2H), 2.97–2.70 (m, 4H) ppm. ^{19}F NMR (377 MHz, CD$_3$CN): $\delta = -81.4$, -113.5 (d, $J = 68.8$ Hz), -122.1 (d, $J = 85.0$ Hz), -123.1, -123.9 (d, $J = 77.8$ Hz), -126.5, -151.4 ppm. ^{13}C NMR (151 MHz, CD$_3$CN): $\delta = 161.4$, 161.1, 159.0, 154.0, 150.7, 139.6, 130.4, 130.3, 128.1, 124.6, 121.8, 116.6, 63.4, 61.5, 31.6 (t, $J = 21.7$ Hz) ppm. HRMS (ESI): calcd. For [C$_{62}$H$_{36}$FeF$_{34}$N$_6$O]$^{2+}$ [$M - $(BF$_4$)$_2$]$^{2+}$: m/z 799.0848; found 799.0855. Anal. Calcd for C$_{62}$H$_{36}$B$_2$F$_{42}$FeN$_6$O$_2$·2 H$_2$O·1.4 C$_2$H$_3$N: C 41.71, H 2.39, N 5.55; found: C 41.74, H 2.44, N 5.51.

Supporting Information

The Supporting Information contains SQUID magnetometry, cyclic voltammetry, spectro-electrochemistry, EPR spectroscopy, DFT calculations, X-ray crystallography, NMR spectroscopy, and polyrized optical microscopy results. Additional references are also cited in there.[55,56]

Conflict of Interests

There are no conflicts to declare.

Data Availability Statement

The data that support the findings of this study are available in the supplementary material of this article.

[1] a) U. S. Schubert, H. Hofmeier, G. R. Newkome, *Modern Terpyridine Chemistry*, Wiley-VCH, Weinheim **2006**; b) H. Hofmeier, U. S. Schubert, *Chem. Soc. Rev.* **2004**, *33*, 373–399.

[2] a) S. Aroua, T. K. Todorova, P. Hommes, L.-M. Chamoreau, H.-U. Reissig, V. Mougel, M. Fontecave, *Inorg. Chem.* **2017**, *56*, 5930–5940; b) P. Hommes, C. Fischer, C. Lindner, H. Zipse, H.-U. Reissig, *Angew. Chem. Int. Ed.* **2014**, *53*, 7647–7651; c) J. R. Colombe, S. Bernhardt, C. Stathakis, S. L. Buchwald, P. Knochel, *Org. Lett.* **2013**, *15*, 5754–5757.

[3] a) S. G. Shepard, S. M. Fatur, A. K. Rappé, N. H. Damrauer, *J. Am. Chem. Soc.* **2016**, *138*, 2949–2952; b) D. G. Brown, N. Sanguantrakun, B. Schulze, U. S. Schubert, C. P. Berlinguette, *J. Am. Chem. Soc.* **2012**, *134*, 12354–12357.

[4] R. Tatikonda, S. Bhowmik, K. Rissanen, M. Haukka, M. Cametti, *Dalton Trans.* **2016**, *45*, 12756–12762.

[5] A. Fermi, G. Bergamini, M. Roy, M. Gingras, P. Ceroni, *J. Am. Chem. Soc.* **2014**, *136*, 6395–6400.

[6] a) Z. Zheng, L. Opilik, F. Schiffmann, W. Liu, G. Bergamini, P. Ceroni, L.-T. Lee, A. Schütz, J. Sakamoto, R. Zenobi, J. VandeVondele, A. D. Schlüter, *J. Am. Chem. Soc.* **2014**, *136*, 6103–6110; b) G. Gröger, W. Meyer-Zaika, C. Böttcher, F. Gröhn, C. Ruthard, C. Schmuck, *J. Am. Chem. Soc.* **2011**, *133*, 8961–8971; c) U. S. Schubert, C. Eschbaumer, *Angew. Chem. Int. Ed.* **2002**, *41*, 2892–2926; d) F. Chen, Y.-K. Tian, Y. Chen, *Chem. Asian J.* **2018**, *13*, 3169–3172.

[7] a) J.-H. Yum, E. Baranoff, F. Kessler, T. Moehl, S. Ahmad, T. Bessho, A. Marchioro, E. Ghadiri, J.-E. Moser, C. Yi, M. K. Nazeeruddin, M. Grätzel, *Nat. Commun.* **2012**, *3*, 631; b) S. A. Sapp, C. M. Elliott, C. Contado, S. Caramori, C. A. Bignozzi, *J. Am. Chem. Soc.* **2002**, *124*, 11215–11222.

[8] a) N. Elgrishi, S. Griveau, M. B. Chambers, F. Bedioui, M. Fontecave, *Chem. Commun.* **2015**, *51*, 2995–2998; b) N. Elgrishi, M. B. Chambers, M. Fontecave, *Chem. Sci.* **2015**, *6*, 2522–2531; c) N. Elgrishi, M. B. Chambers, V. Artero, M. Fontecave, *Phys. Chem. Chem. Phys.* **2014**, *16*, 13635–13644.

[9] R. Tatikonda, M. Cametti, E. Kalenius, A. Famulari, K. Rissanen, M. Haukka, *Eur. J. Inorg. Chem.* **2019**, *2019*, 4463–4470.

[10] K. Kuroiwa, T. Arie, S. Sakurai, S. Hayami, T. J. Deming, *J. Mater. Chem. C* **2015**, *3*, 7779–7783.

[11] S. Hayami, R. Moriyama, Y. Shigeyoshi, R. Kawajiri, T. Mitani, M. Akita, K. Inoue, Y. Maeda, *Inorg. Chem.* **2005**, *44*, 7295–7297.

[12] a) M. A. Halcrow, *Chem. Soc. Rev.* **2011**, *40*, 4119–4142; b) M. A. Halcrow, *Spin-Crossover Materials: Properties and Application*, Wiley, Chichester **2013**; c) P. Gütlich, A. Hauser, H. Spiering, *Angew. Chem. Int. Ed.* **1994**, *33*, 2024–2054; d) P. Guionneau, M. Marchivie, G. Bravic, J.-F. Létard, D. Chasseau, *J. Mater. Chem.* **2002**, *12*, 2546–2551; e) A. B. Gaspar, M. C. Muñoz, V. Niel, J. A. Real, *Inorg. Chem.* **2001**, *40*, 9–10; f) J. Zarembowitch, O. Kahn, *Inorg. Chem.* **1984**, *23*, 589–593; g) F. Fürmeyer, D. Münzberg, L. M. Carrella, E. Rentschler, *Molecules* **2020**, *25*, 855; h) N. M. J. Nik Ibrahim, S. M. Said, A. Mainal, M. F. Mohd Sabri, N. Abdullah, M. M. I. Megat Hasnan, H. Che Hassan, M. F. Mohd Salleh, W. A. Wan Mohd Mahiyiddin, *Mater. Res. Bull.* **2020**, *126*, 110828; i) M. Griffin, S. Shakespeare, H. J. Shepherd, C. J. Harding, J.-F. Létard, C. Desplanches, A. E. Goeta, J. A. K. Howard, A. K. Powell, V. Mereacre, Y. Garcia, A. D. Naik, H. Müller-Bunz, G. G. Morgan, *Angew. Chem. Int. Ed.* **2011**, *50*, 896–900; j) W. Phonsri, B. A. I. Lewis, G. N. L. Jameson, K. S. Murray, *Chem. Commun.* **2019**, *55*, 14031–14034; k) C. Cook, F. Habib, T. Aharen, R. Clérac, A. Hu, M. Murugesu, *Inorg. Chem.* **2013**, *52*, 1825–1831.

[13] a) P. Silva, S. M. F. Vilela, J. P. C. Tomé, F. A. Almeida Paz, *Chem. Soc. Rev.* **2015**, *44*, 6774–6803; b) C.-L. Ho, Z.-Q. Yu, W.-Y. Wong, *Chem. Soc. Rev.* **2016**, *45*, 5264–5295; c) M. Castellano, R. Ruiz-García, J. Cano, J. Ferrando-Soria, E. Pardo, F. R. Fortea-Pérez, S.-E. Stiriba, W. P. Barros, H. O. Stumpf, L. Cañadillas-Delgado, J. Pasán, C. Ruiz-Pérez, G. de Munno, D. Armentano, Y. Journaux, F. Lloret, M. Julve, *Coord. Chem. Rev.* **2015**, *303*, 110–138; d) M. K. Singh, Y. Yang, C. G. Takoudis, *Coord. Chem. Rev.* **2009**, *253*, 2920–2934; e) E. Chelebaeva, J. Larionova, Y. Guari, R. A. S. Ferreira, L. D. Carlos, F. A. A. Paz, A. Trifonov, C. Guérin, *Inorg. Chem.* **2009**, *48*, 5983–5995; f) J. Long, J. Rouquette, J. M. Thibaud, R. A. Ferreira, L. D. Carlos, B. Donnadieu, V. Vieru, L. F. Chibotaru, L. Konczewicz, J. Haines, Y. Guari, J. Larionova, *Angew. Chem. Int. Ed.* **2015**, *54*, 2236–2240.

[14] S. Hayami, R. Moriyama, A. Shuto, Y. Maeda, K. Ohta, K. Inoue, *Inorg. Chem.* **2007**, *46*, 7692–7694.

[15] R. Akiyoshi, Y. Hirota, D. Kosumi, M. Tsutsumi, M. Nakamura, L. F. Lindoy, S. Hayami, *Chem. Sci.* **2019**, *10*, 5843–5848.

[16] a) M. Seredyuk, A. B. Gaspar, V. Ksenofontov, Y. Galyametdinov, J. Kusz, P. Gütlich, *Adv. Funct. Mater.* **2008**, *18*, 1089–2101; b) M. Seredyuk, A. B. Gaspar, V. Ksenofontov, Y. Galyametdinov, J. Kusz, P. Gütlich, *J. Am. Chem. Soc.* **2008**, *130*, 1431–1439; c) A. B. Gaspar, M. Seredyuk, P. Gütlich, *Coord. Chem. Rev.* **2009**, *253*, 2399–2413.

[17] a) A. B. Gaspar, V. Ksenofontov, M. Seredyuk, P. Gütlich, *Coord. Chem. Rev.* **2005**, *249*, 2661–2676; b) S. Bonhommeau, P. G. Lacroix, D. Talaga, A. Bousseksou, M. Seredyuk, I. O. Fritsky, V. Rodriguez, *J. Phys. Chem. C* **2012**, *116*, 11251–11255; c) W. Liu, X. Bao, L.-L. Mao, J. Tucek, R. Zboril,

Chemistry–A European Journal

Research Article
doi.org/10.1002/chem.202301246

Chemistry
Europe
European Chemical
Societies Publishing

J.-L. Liu, F.-S. Guo, Z.-P. Ni, M.-L. Tong, *Chem. Commun.* **2014**, *50*, 4059–4061.

[18] a) I. Suleimanov, O. Kraieva, J. Sánchez Costa, I. O. Fritsky, G. Molnár, L. Salmon, A. Bousseksou, *J. Mater. Chem. C* **2015**, *3*, 5026–5032; b) A. Santoro, L. J. Kershaw Cook, R. Kulmaczewski, S. A. Barrett, O. Cespedes, M. A. Halcrow, *Inorg. Chem.* **2015**, *54*, 682–693; c) C. F. Wang, R. F. Li, X. Y. Chen, R. J. Wei, L. S. Zheng, J. Tao, *Angew. Chem. Int. Ed.* **2015**, *54*, 1574–1577; d) M. Estrader, J. S. Uber, L. A. Barrios, J. Garcia, P. Lloyd-Williams, O. Roubeau, S. J. Teat, G. Aromi, *Angew. Chem. Int. Ed.* **2017**, *56*, 15622–15627; e) J.-Y. Ge, Z. Chen, L. Zhang, X. Liang, J. Su, M. Kurmoo, J.-L. Zuo, *Angew. Chem. Int. Ed.* **2019**, *58*, 8789–8793; f) B. Benaicha, K. Van Do, A. Yangui, N. Pittala, A. Lusson, M. Sy, G. Bouchez, H. Fourati, C. J. Gómez-García, S. Triki, K. Boukheddaden, *Chem. Sci.* **2019**, *10*, 6791–6798.

[19] a) S. Hayami, Y. Shigeyoshi, M. Akita, K. Inoue, K. Kato, K. Osaka, M. Takata, R. Kawajiri, T. Mitani, Y. Maeda, *Angew. Chem. Int. Ed.* **2005**, *44*, 4899–4903; b) J. A. Kitchen, N. G. White, C. Gandolfi, M. Albrecht, G. N. L. Jameson, J. L. Tallon, S. Brooker, *Chem. Commun.* **2010**, *46*, 6464–6466.

[20] a) S. Hayami, K. Murata, D. Urakami, Y. Kojima, M. Akita, K. Inoue, *Chem. Commun.* **2008**, *48*, 6510–6512; b) S. Hayami, D. Urakami, Y. Kojima, H. Yoshizaki, Y. Yamamoto, K. Kato, A. Fuyuhiro, S. Kawata, K. Inoue, *Inorg. Chem.* **2010**, *49*, 1428–1432; c) S. Hayami, Y. Komatsu, T. Shimizu, H. Kamihata, Y. H. Lee, *Coord. Chem. Rev.* **2011**, *255*, 1981–1990; d) Y. Komatsu, K. Kato, Y. Yamamoto, H. Kamihata, Y. H. Lee, A. Fuyuhiro, S. Kawata, S. Hayami, *Eur. J. Inorg. Chem.* **2012**, 2769–2775; e) S. Hayami, M. Nakaya, H. Ohmagari, A. S. Alao, M. Nakamura, R. Ohtani, R. Yamaguchi, T. Kuroda-Sowa, J. K. Clegg, *Dalton Trans.* **2015**, *44*, 9345–9348.

[21] S. Hayami, K. Kato, Y. Komatsu, A. Fuyuhiro, M. Ohba, *Dalton Trans.* **2011**, *40*, 2167–2169.

[22] a) A. B. Lindstrom, M. J. Strynar, E. L. Libelo, *Environ. Sci. Technol.* **2011**, *45*, 7954–7961; b) A. Zaggia, L. Conte, L. Falletti, M. Fant, A. Chiorboli, *Water Res.* **2016**, *91*, 137–146; c) R. A. Dickman, D. S. Aga, *J. Hazard. Mater.* **2022**, *436*, 129120; d) H. Li, A. L. Junker, J. Wen, L. Ahrens, M. Sillanpää, J. Tian, F. Cui, L. Vergeynst, Z. Wei, *J. Chem. Eng.* **2023**, *452*, 139202.

[23] a) A. K. Greaves, R. J. Letcher, *Chemosphere* **2013**, *93*, 574–580; b) M. Cornelsen, R. Weber, S. Panglisch, *Emerg. Contam.* **2021**, *7*, 63–76.

[24] L. Arnedo-Sánchez, Nonappa, S. Bhowmik, S. Hietala, K. Rissanen, M. Lahtinen, L. De Cola, K. Rissanen, *Dalton Trans.* **2017**, *46*, 7309–7316.

[25] D. Shao, L. Shi, L. Yin, B.-L. Wang, Z.-X. Wang, Y.-Q. Zhang, X.-Y. Wang, *Chem. Sci.* **2018**, *9*, 7986–7991.

[26] C. J. Gorter, J. H. van Vleck, *Phys. Rev.* **1947**, *72*, 1128–1129.

[27] N. Bloembergen, E. M. Purcell, R. V. Pound, *Phys. Rev.* **1948**, *73*, 679–712.

[28] a) J. H. Van Vleck, *Phys. Rev.* **1948**, *74*, 1168–1183; b) P. W. Anderson, P. R. Weiss, *Rev. Mod. Phys.* **1953**, *25*, 269–276; c) P. W. Anderson, *Phys. Rev.* **1951**, 342.

[29] a) V. A. Atsarkin, G. A. Vasneva, V. V. Demidov, F. S. Dzheparov, B. M. Odintsov, R. B. Clarkson, *JETP Lett.* **2000**, *72*, 369–372; b) L. Tagirov, *IEEE Trans. Magn.* **1987**, *23*, 2230–2232.

[30] a) P. Sati, A. Stepanov, V. Pashchenko, *Low Temp. Phys.* **2007**, *33*, 927–930; b) A. L. Pérez, A. Kemmerer, M. A. Rey, S. D. Dalosto, C. A. Ramos, M. C. G. Passeggi, A. C. Rizzi, C. D. Brondino, *Eur. J. Inorg. Chem.* **2018**, 4604–4613.

[31] a) A. C. Rizzi, N. I. Neuman, P. J. González, C. D. Brondino, *Eur. J. Inorg. Chem.* **2016**, 192–207; b) N. I. Neuman, E. Burna, R. Baggio, M. C. G. Passeggi, A. C. Rizzi, C. D. Brondino, *Inorg. Chem. Front.* **2015**, *2*, 837–845.

[32] a) M. Nößler, R. Jäger, D. Hunger, M. Reimann, T. Bens, N. I. Neuman, A. S. Hazari, M. Kaupp, J. van Slageren, B. Sarkar, *Eur. J. Inorg. Chem.* **2023**, e202300091; b) F. Stein, M. Nößler, A. S. Hazari, L. Böser, R. Walter, H. Liu, E. Klemm, B. Sarkar, *Chem. Eur. J.* **2023**, *29*, e202300405.

[33] O. A. Oyetade, V. O. Nyamori, B. S. Martincigh, S. B. Jonnalagadda, *RSC Adv.* **2016**, *6*, 2731–2745.

[34] P. Gütlich, H. A. Goodwin, *Spin Crossover in Transition Metal Compounds I, II, and III*, Springer, Berlin **2004**.

[35] R. J. Davidson, E. W. Ainscough, A. M. Brodie, G. B. Jameson, M. R. Waterland, H. R. Allcock, M. D. Hindenlang, B. Moubaraki, K. S. Murray, K. C. Gordon, R. Horvath, G. N. L. Jameson, *Inorg. Chem.* **2012**, *51*, 8307–8316.

[36] A. Ondo, T. Ishida, *Crystals* **2018**, *8*, 155.

[37] a) J. A. Real, A. B. Gaspar, M. C. Muñoz, *Dalton Trans.* **2005**, *12*, 2062–2079; b) O. Sato, J. Tao, Y.-Z. Zhang, *Angew. Chem. Int. Ed.* **2007**, *46*, 2152–2187; c) M. A. Halcrow, *Chem. Soc. Rev.* **2011**, *40*, 4119–4142.

[38] a) J. England, E. Bill, T. Weyhermüller, F. Neese, M. Atanasov, K. Wieghardt, *Inorg. Chem.* **2015**, *54*, 12002–12018; b) J. England, C. C. Scarborough, T. Weyhermüller, S. Sproules, K. Wieghardt, *Eur. J. Inorg. Chem.* **2012**, 4605–4621.

[39] a) P. Nielsen, H. Toftlund, A. D. Bond, J. F. Boas, J. R. Pilbrow, G. R. Hanson, C. Noble, M. J. Riley, S. M. Neville, B. Moubaraki, K. S. Murray, *Inorg. Chem.* **2009**, *48*, 7033–7047; b) S. Kremer, W. Henke, D. Reinen, *Inorg. Chem.* **1982**, *21*, 3013–3022.

[40] S. Ye, *MRL* **2023**, *3*, 43–60.

[41] B. R. McGarvey, *Can. J. Chem.* **1975**, *53*, 2498–2511.

[42] a) R. Calvo, C. A. Steren, O. E. Piro, T. Rojo, F. J. Zuniga, E. E. Castellano, *Inorg. Chem.* **1993**, *32*, 6016–6022; b) N. I. Neuman, V. G. Franco, F. M. Ferroni, R. Baggio, M. C. G. Passeggi, A. C. Rizzi, C. D. Brondino, *J. Phys. Chem. A* **2012**, *116*, 12314–12320; c) A. L. Pérez, N. I. Neuman, R. Baggio, C. A. Ramos, S. D. Dalosto, A. C. Rizzi, C. D. Brondino, *Polyhedron* **2017**, *123*, 404–410.

[43] a) F. Neese, *WIREs Comput. Mol. Sci.* **2012**, *2*, 73–78; b) F. Neese, *WIREs Comput. Mol. Sci.* **2018**, *8*, e1327; c) F. Neese, *WIREs Comput. Mol. Sci.* **2022**, *12*, e1606.

[44] D. Venegas-Yazigi, K. A. Brown, A. Vega, R. Calvo, C. Aliaga, R. C. Santana, R. Cardoso-Gil, R. Kniep, W. Schnelle, E. Spodine, *Inorg. Chem.* **2011**, *50*, 11461–11471.

[45] G. R. Fulmer, A. J. M. Miller, N. H. Sherden, H. E. Gottlieb, A. Nudelman, B. M. Stoltz, J. E. Bercaw, K. I. Goldberg, *Organometallics* **2010**, *29*, 2176–2179.

[46] M. Krejčik, M. Daněk, F. Hartl, *J. Electroanal. Chem.* **1991**, *317*, 179–187.

[47] a) G. M. Sheldrick, *SHELXS-97, Program for Crystal Structure Solution and Refinement* **1997**, University of Göttingen, Germany; b) G. Sheldrick, *Acta Crystallogr. Sect. A* **2008**, *64*, 112–122; c) G. M. Sheldrick, *SADABS Ver. 2008/1, SADABS. Program for Empirical Absorption Correction* **2012**, University of Göttingen, Germany; d) G. M. Sheldrick, *SHELXL Version 2014/7, Program for Chrystal Structure Solution and Refinement* **2014**, University of Göttingen, Germany; e) G. Sheldrick, *Acta Crystallogr. Sect. C* **2015**, *71*, 3–8; f) A. Spek, *J. Appl. Crystallogr.* **2003**, *36*, 7–13; g) SAINT+, *Data Integration Engine, Version 8.27b©*, Bruker AXS, Madison, Wisconsin, USA **1997–2012**.

[48] G. A. Bain, J. F. Berry, *J. Chem. Educ.* **2008**, *85*, 532.

[49] a) V. N. Staroverov, G. E. Scuseria, J. Tao, J. P. Perdew, *J. Chem. Phys.* **2003**, *119*, 12129–12137; b) J. Tao, J. P. Perdew, V. N. Staroverov, G. E. Scuseria, *Phys. Rev. Lett.* **2003**, *91*, 146401.

[50] F. Weigend, R. Ahlrichs, *Phys. Chem. Chem. Phys.* **2005**, *7*, 3297–3305.

[51] M. M. Quintal, A. Karton, M. A. Iron, A. D. Boese, J. M. L. Martin, *J. Phys. Chem. A* **2006**, *110*, 709–716.

[52] a) S. K. T. Petrenko, F. Neese, *J. Chem. Phys.* **2011**, *134*, 54116; b) F. Neese, G. Olbrich, *Chem. Phys. Lett.* **2002**, *362*, 170–178; c) R. Izsák, F. Neese, *J. Chem. Phys.* **2011**, *135*, 144105; d) J. L. Whitten, *J. Chem. Phys.* **1973**, *58*, 4496–4501; e) O. Vahtras, J. Almlöf, M. W. Feyereisen, *Chem. Phys. Lett.* **1993**, *213*, 514–518; f) F. Neese, F. Wennmohs, A. Hansen, U. Becker, *Chem. Phys.* **2009**, *356*, 98–109.

[53] a) K. Eichkorn, O. Treutler, H. Öhm, M. Häser, R. Ahlrichs, *Chem. Phys. Lett.* **1995**, *240*, 283–290; b) K. Eichkorn, F. Weigend, O. Treutler, R. Ahlrichs, *Theor. Chem. Acc.* **1997**, *97*, 119–124; c) F. Weigend, *Phys. Chem. Chem. Phys.* **2006**, *8*, 1057–1065.

[54] a) D. Prescher, T. Thiele, R. Ruhmann, *J. Fluorine Chem.* **1996**, *79*, 145–148; b) J. Rábai, D. Szabó, E. K. Borbás, I. Kövesi, I. Kövesdi, A. Csámpai, Á. Gömöry, V. E. Pashinnik, Y. G. Shermolovich, *J. Fluorine Chem.* **2002**, *114*, 199–207.

[55] K. Yamaguchi, Y. Takahara, T. Fueno, *Applied Quantum Chemistry*, Springer Dordrecht, D. Reidel Publishing Company, Dordrecht, Holland **1986**.

[56] T. Soda, Y. Kitagawa, T. Onishi, Y. Takano, Y. Shigeta, H. Nagao, Y. Yoshioka, K. Yamaguchi, *Chem. Phys. Lett.* **2000**, *319*, 223–230.